Dissertação N°456

Química Mineral de Magnetita e Assinatura Isotópica de Enxofre em Sulfetos de Cu-Fe: Implicações para o Modelo Evolutivo do depósito tipo IOCG Metamorfizado do Salobo, Província Mineral de Carajás.

Yuri Tatiana Campo Rodríguez

Universidade de Brasília

Instituto de Geociências

Brasília

2020

Química Mineral de Magnetita e Assinatura Isotópica de Enxofre em Sulfetos de Cu-Fe: Implicações para o Modelo Evolutivo do depósito tipo IOCG Metamorfizado do Salobo, Província Mineral de Carajás.

Aluna: Yuri Tatiana Campo Rodríguez

Matrícula: 18/0060104

Orientadora: Prof. Dra. Maria Emília Schutesky Della Giustina

Dissertação de Mestrado Apresentada ao Instituto de Geociências da UnB para Obtenção do Título de Mestre(a) em Geologia na Área de Concentração Geoquímica

Universidade de Brasília

Instituto de Geociências

Brasília

2020

O presente trabalho foi realizado com apoio da Coordenação de Aperfeiçoamento de Pessoal de Nível Superior - Brasil (CAPES) – Código de Financiamento 001, e do Conselho Nacional de Desenvolvimento Científico e Tecnológico do Brasil CNPq.

Ficha catalográfica elaborada automaticamente,
com os dados fornecidos pelo(a) autor(a)

Campo Rodríguez, Yuri Tatiana
Ct THE GIANT METAMORPHOSED IOCG SALOBO DEPOSIT, CARAJAS MINERAL PROVINCE: MAGNETITE TRACE ELEMENT CHALCOPYRITE PYRITE S ISOTOPES EVIDENCES FOR A MULTIPLE-STAGE EVOLUTIONARY MODEL / Yuri Tatiana Campo Rodríguez; orientador Maria Emilia Schutesky Della Giustina. -- Brasília, 2020.
72 p.

Tese (Doutorado - Mestrado em Geologia) -- Universidade de Brasília, 2020.

1. Processos magmático-hidrotermais formaram a magnetita do deposito de Salobo.. 2. Os isótopos S corroboram uma fonte magmática de enxofre.. 3. A formação dos sulfetos de Cu-Fe poderia ter sido causada pela desproporção do enxofre induzida pela cristalização da magnetita.. I. Schutesky Della Giustina, Maria Emilia, orient. II. Título.

Agradecimentos

À Deus.

À minha fiei e amada família: Yesid, Cony, Ana e Juan por ser esse apoio que incansavelmente permanece ao meu lado.

À minha orientadora Prof. Dra. Maria Emillia Schutesky, por me aceitar como sua pupila me confiando este trabalho tão importante para os meus interesses acadêmicos, e principalmente por seu constante conselho para o bom desenvolvimento desse trabalho.

Ao Prof. Dr. Claudinei Gouveia pelo conselho e acompanhamento nestes dois anos de estudo.

Ao Dr Matin Whitehouse pelas análises de isótopos.

Agradeço também a todos que me acompanharam nesse estudo, professores e administrativos da universidade de Brasília e amigos: Marcel, Caro, Naza e Seba em especial.

À Hetiene por ser essa mão amiga.

À Marina por sempre me escutar.

Ao Karatê Kyokushin por fomentar em mim a disciplina, sem a qual eu não poderia ter realizado esse trabalho.

Agradeço ao CNPq e a CAPES pela concessão das bolsas de mestrado tanto para brasileiros como para estrangeiros.

À empresa de mineração VALE.

Para Ana e Juan…

«… Los que un tiempo creyeron que mi inteligencia irradiaría extraordinariamente, cual una aureola de mi juventud; los que se olvidaron de mi apenas mi planta descendió al infortunio; los que al recordarme alguna vez piensen en mi fracaso y se pregunten por qué no fui lo que pude haber sido, sepan que el destino implacable me desarraigó de la prosperidad incipiente y me lanzó a las pampas, para que ambulara, vagabundo, como los vientos y me extinguiera como ellos sin dejar más que ruido y desolación».

La Voragine

Resumo

Os depósitos tipo IOCG são formados por fluidos magmático-hidrotermais com forte controle estrutural, e são ricos em óxidos de Fe e sulfetos de Cu-Fe precedidos por alteração hidrotermal sódico-cálcica. No entanto, modelos conceituais ainda não esclarecem se a fonte de enxofre deriva da mesma fonte do magma ou apresenta contribuições de fontes externas, e quais processos hidrotermais geram o enriquecimento em óxido de ferro no depósito. Além disso, modelos atuais não estabelecem um paralelo quando comparado a outros tipos de depósitos de cobre magmáticos de alta temperatura. O principal depósito IOCG do Brasil, o depósito do Salobo localiza-se na Província Mineral de Carajás, sudeste do Cráton Amazônico. Contém recursos de 986 Mt a 0,82% Cu e 0,49 g/t Au. O minério é caraterizado por um alto teor de sulfetos de cobre (bornita e calcocita) hospedados em rochas ricas em magnetita as quais apresentam metamorfismo-deformação e alteração hidrotermal sobreposta. Diversos eventos geológicos como metamorfismo Neoarqueno associado à atividade da zona de Cizalhamente de Cinzento e alterações hidrotermais produto de magmatismo Paleoproterozoico tem dificultado interpretações geoquímicas e da origem do minério no depósito.

À parte de discussões relacionadas à geocronologia desse depósito, este estudo tem o objetivo de contribuir para melhor compreensão do modelo evolutivo da mineralização primária, a partir da combinação de análises texturais e mineralógicas de óxidos com isótopos de enxofre em sulfetos de Cu e Fe. Os estudos mineralógicos indicam que há pelo menos três episódios de formação de magnetita. A primeira magnetita (Mgt tipo I) rica em Pb (média 884 ppm), antecede a formação dos sulfetos constituindo a matriz de uma brecha composta por silicatos ricos em Fe (Ferrosilita, Faialita e Hastingsita). A segunda geração (Mgt tipo II) é rica em inclusões de Apatita, Calcopirita, Pirita e Monazita, e ocorre como xenocristais em brechas cimentadas por calcopirita, refletido em maiores concentrações de Cu (média 712 ppm). A terceira fase (Mgt tipo III) constitui um agregado granoblástico em xistos miloníticos ricos em magnetita com altos valores de V (média 503 ppm). No entanto, os padrões composicionais não apresentam um zoneamento geoquímico nem distinção entre os três tipos de magnetita quando analisados em diagramas discriminantes.

Os dados isotópicos revelaram um intervalo no $\delta^{34}S_{V\text{-}CDT}$ de 0,88 a 5,04 ‰ que em conjunto com as associações texturais da calcopirita relacionada a Mgt I e II apontam para uma fonte de enxofre principalmente magmática sem/ou com contribuições mínimas de fluidos altamente salinos externos e indicam um processo de desproporcionalização do enxofre na formação inicial dos sulfetos. Portanto, nossos resultados suportam os tipos de magnetita I e II foram formados a partir de um fluido magmático-hidrotermal oxidado rico em Cu em evolução durante o magmatismo Neoarqueano (anterior à ~2,5 Ga), sob condições atmosféricas não oxidantes. Além disso a oxidação no sistema provocada pela cristalização da magnetita desencadeou a desproporcionalização do enxofre no fluido de caráter magmático-hidrotermal, assim a redução do sulfato contido nesse fluido resultou na formação dos sulfetos de cobre, ou seja, na formação da mineralização de Cu-Au nas brechas de calcopirita (Mgt tipo II), a qual também teve uma contribuição em Cu pela substituição de pirita por calcopirita.

O metamorfismo/metasomatismo subsequente de baixo grau associado ao *emplacement* do Granito Old Salobo e à reativação da Zona de Cisalhamento Cinzento em ~ 2,5 Ga resultou em uma recristalização de magnetita (Mgt tipo III). Finalmente, um magmatismo granítico regional volumoso do tipo A durante o Paleoproterozoico produziu uma remobilização e reconcentração dos sulfetos de Cu, resultando em veios de caráter rúptil e discordantes, de bornita, digenita, covelita e calcocita, além de texturas de exsoluções de minerais de baixa temperatura. Durante esse evento de remobilização não se produziu um novo crescimento de magnetita.

Palavras-chave: Depósitos IOCG, isótopos de enxofre, química de magnetita, desproporcionalização do enxofre.

Abstract

The genesis of IOCG deposits has been intensely debated, in particular, conceptual models are not yet clear whether the sulfur source is derived from the same magma source or have external contributions and which hydrothermal processes create the iron oxide enrichment. The Salobo deposit is a world-class iron oxide copper and gold (IOCG) deposit located in the Carajás Mineral Province, southeastern Amazon Craton, Brazil. It contains resources of 986 Mt @ 0.82% Cu and 0.49 g/t Au. The ore is characterized by a high tenor of copper-sulfides (bornite and chalcocite) hosted in magnetite-rich rocks with superimposed hydrothermal alteration and metamorphism-deformation, which have complicated ore-genesis and the geochemical interpretations.

In this study, we combine mineralogical and chemical analysis of magnetite with sulfur isotopes on Cu-Fe sulfides of the Salobo deposit. Mineralogical studies show that there are three magnetite types, including massive, pristine to inclusion-poor *magnetite breccia* (Mgt type I), inclusion-rich *magnetite-bearing breccia* (Mgt type II), and the granoblastic *magnetite schist* (Mgt type III). The Mgt type I is characterized by an association with high-temperature Fe-rich silicate minerals (i.e., ferrosilite, fayalite, and hastingsite), whereas the Mgt type II is associated with Cu-Fe sulfides relate to chalcopyrite-rich breccias. The Mgt type III is related to the mylonitic schist crosscutted by discordant veins of low-temperature Cu-Fe sulfides. In general, the trace element composition of these magnetite populations is similar without display a distinctive geochemical trend in discrimination diagrams.

Thus, the Mgt type III represents recrystallization possible of the other magnetite types during Neoarchean metamorphism/metasomatism with an overprint of magmatic-hydrothermal alteration during the Paleoproterozoic. The range in $\delta^{34}S_{V\text{-}CDT}$ of 0.88 to 5.04‰ is consistent with a magmatic-hydrothermal sulfur source without/or minimal external contributions and indicates a sulfur disproportionation process in the early sulfide formation. Therefore, our data support that the magnetite types I and II were formed from an evolving oxidized-magmatic-hydrothermal Cu-rich fluid, under non-oxidizing atmospheric conditions. Moreover, the magnetite oxidation (crystallization) triggered the sulfur disproportionation, thus the sulfate reduction and the sulfide formation. Subsequent low-grade metamorphism associated with the emplacement of the

Old Salobo Granite and reactivation of the Cinzento Shear Zone in ca. ~2.5 Ga resulted in the recrystallized Mgt type, which subsequently underwent hydrothermal alteration as a result of Paleoproterozoic magmatism.

Keywords: Iron oxide copper-gold, Sulfur isotopes, Magnetite chemistry, Sulfur disproportionation.

Índice

Introdução, Justificativa e Objetivos

Um dos depósitos mais atraentes na exploração de Cu-Au são os de óxido de ferro-cobre-ouro (*Iron oxide-copper-gold,* doravante IOCG) de classe mundial, graças a seus altos teores de Cu e Au (Williams et al., 2005). Em todo o mundo os depósitos IOCG compartilham aspectos similares quanto ao ambiente geológico e associação mineral. Em geral, os IOCG comumente são encontrados com uma ampla distribuição no espaço e no tempo, desde ambientes pós-orogênicos do Neoarqueano (por exemplo, distrito de Carajás, Brasil) e Proterozóico (por exemplo, Olympic Damn, Austrália; Great Bear, Canadá), até Mesozóico, na margem continental ativa da Cordilheira Andina (por exemplo, Candelaria e Punta del Cobre, Chile; Sillitoe 2003; Williams et al. 2005; Richards and Mumin 2013; Fig. 1).

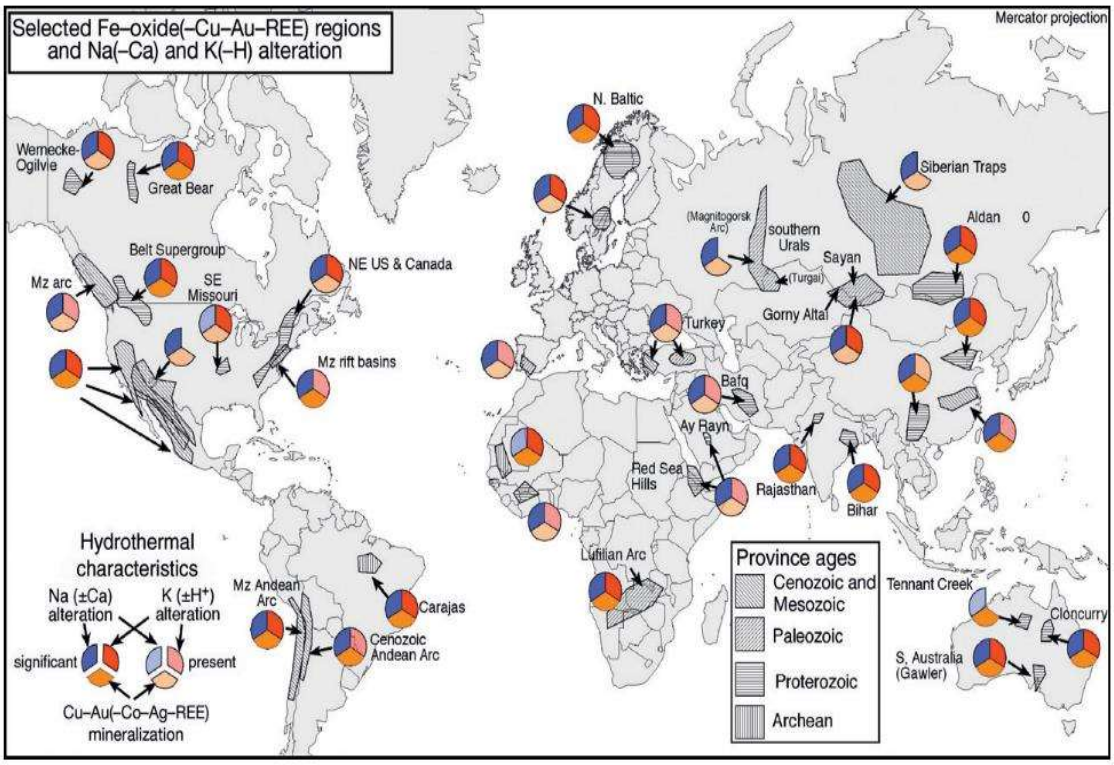

Fig. 1. Localização das principais províncias de IOCG e de outras províncias hidrotermais de óxido de Fe com depósitos seleccionados. Para cada província, os símbolos circulares de três partes indicam a presença conhecida de metais e os principais tipos de alterações hidrotermais. Tomado de (Barton, 2014).

Além disso, as mineralizações do tipo IOCG são formados por fluidos magmático-hidrotermais ricos em Fe, constituindo zonas de alteração hidrotermais volumetricamente

extensas com importante controle estrutural (Richards and Mumin, 2013; Williams et al., 2005). Na área dominada pela magnetita, são mais comuns as alterações de mais alta temperatura (Na-Ca e K), enquanto a área dominada pela hematita está relacionada a zonas mais rasas, associadas à cloritização e sericitização (Williams et al., 2005). As diferentes condições de fO_2 - fS_2 podem formar minério caracterizado por calcopirita, bornita e calcocita e pobres em pirita (por exemplo, Salobo, Brasil; Olympic Damn, Austrália) e outras nos quais a pirita e calcopirita são os principais sulfetos (por exemplo, Candelária, Chile; Williams et al. 2005). Depósitos IOCG metamorfizados, entretanto, apresentam distintos zoneamentos da mineralização sequências de alterações hidrotermais, em parte por estarem preservados em cinturões com deformação frágil-dúctil sobreposta (e.g., Great Bear, Canada (Acosta-Góngora et al., 2018); Salobo, Brazil (Schutesky and Gouveia de Oliveira, *accepted*; Vieira et al., 2019); Norrbotten, Sweden (Gleeson and Smith, 2009; Storey and Smith, 2017).

A ampla gama de características geológicas dos depósitos IOCG tem dificultado a definição de um modelo genético comum, especialmente que explique a origem dos fluidos, metais e enxofre responsáveis pela mineralização de Cu-Au (Gleeson and Smith 2009; Richards and Mumin 2013; Storey and Smith 2017; Acosta-Góngora et al. 2018; entre outros). No entanto, os modelos metalogenéticos atuais consideram que o fluido mineralizante pode ter fontes diferentes e seus componentes podem ser alterados através de vários processos durante sua evolução. Numerosos estudos de inclusões fluidas associadas a isótopos radiogênicos (por exemplo, Re-Os, Ar-Ar, Sm-Nd) e estáveis (por exemplo, $\delta^{18}O$, $\delta^{34}S$, $\delta^{65}Cu$, $\delta^{37}Cl$) tem demostrado uma origem magmática-hidrotermal envolvendo fluidos magmáticos primários, embora com contribuições variáveis por remobilização de rochas encaixantes (Acosta-Góngora et al., 2018; Richards and Mumin, 2013; Schlegel et al., 2017; Storey and Smith, 2017). Adicionalmente, autores consideram ainda uma contribuição a partir de salmouras superficiais e possíveis fluidos meta-evaporíticos (Xavier et al., 2008), como em depósitos IOCG andinos (e.g., El Laco; Barton and Johnson (1996), Candelaria e Raúl Condestable; Chiaradia et al. (2006)).

Modelos conceituais sobre a formação de mineralizações tipo IOCG (Barton, 2014; Chen, 2013; Pollard, 2006; Williams et al., 2010, 2005) que envolvem uma fonte magmática de enxofre (Acosta-Góngora et al., 2018; Pollard, 2006; Schlegel et al., 2017) sugerem que os óxidos de ferro associados a sulfetos de Cu-Fe refletem uma mineralização pobre em enxofre que normalmente requere uma contribuição oxidada,

enriquecida em sulfato (Barton, 2014; Hitzman et al., 1992; Richards and Mumin, 2013; Williams et al., 2005). A redução de enxofre é de crítica importância para a precipitação do minério sulfetado de Cu (Barton, 2014; Williams et al., 2005), e pode ser gerada i) pela redução de sulfato (Barton, 2014), ii) pela remobilização do enxofre de sulfetos pré-existentes, como a pirita (Schlegel et al. 2017 e referências contidas) ou iii) pela adição de enxofre a partir de um fluido externo (Chen, 2013). Para depósitos de cobre do tipo pórfiro os modelos metalogenéticos são melhor compreendidos. Nesse caso, tem se proposto que a cristalização de magnetita é o processo principal para a redução de sulfato em magmas oxidados, o qual implica na oxidação de ferro ferroso (Sun et al., 2015, 2013).

Tendo em vista que a composição do magma ou de soluções hidrotermais ao longo do caminho do fluxo mineralizante controla a composição dos elementos traço em magnetita (Dare et al., 2014; Nadoll et al., 2014), foi proposta a utilização desse mineral como traçadores, sendo útil para a distinção entre diferentes depósito minerais contendo óxidos de ferro, bem como dos processos primários de formação do minério (Dare et al., 2014; Dupuis and Beaudoin, 2011; Knipping et al., 2015; Nadoll et al., 2014; Wang et al., 2018). Portanto, caracterizar a química de magnetita em relação à fonte de fluido é crucial para compreender e discutir o modelo genético para um depósito do tipo IOCG.

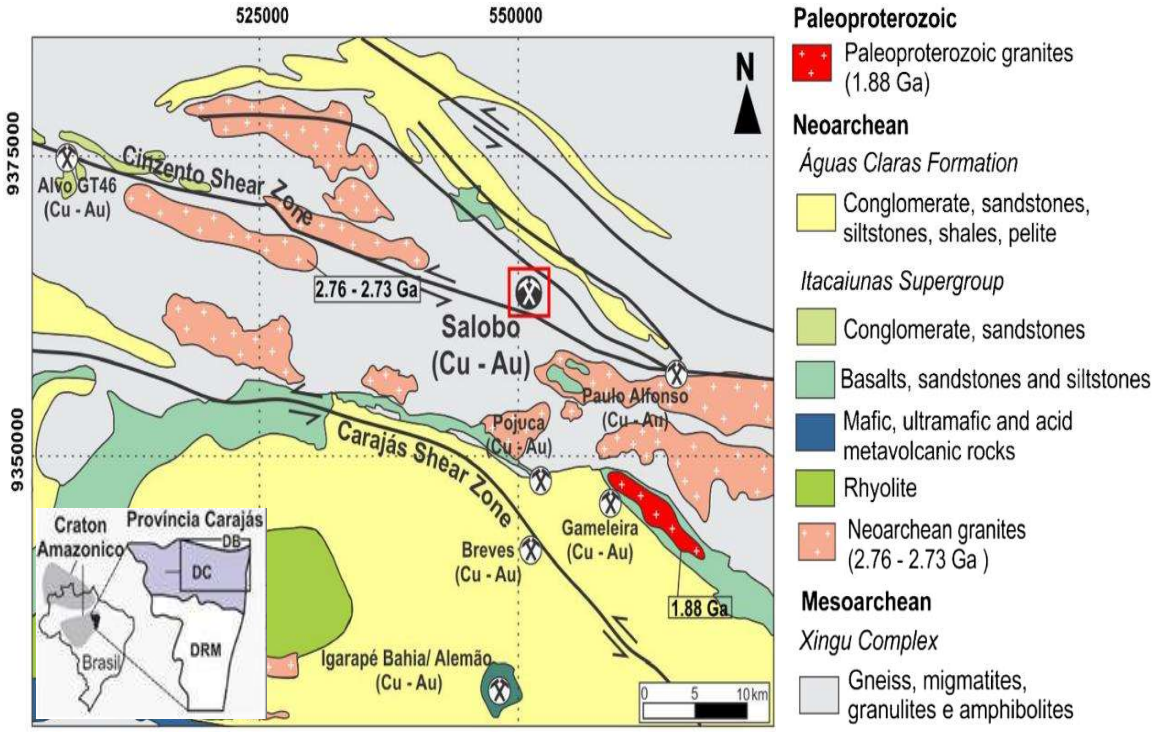

Fig. 2. Mapa geológico simplificado do norte do Domínio de Carajás com a localização do depósito de Salobo IOCG e as principais zonas de cisalhamento. Modified from Melo et al. (2017).

No Brasil, os IOCG se encontram localizados na Província Mineral de Carajás (PMC) no estado do Pará, sudeste do Cráton Amazônico, e constitui o segmento crustal mais antigo desse cráton (Vasquez et al. 2008). A PMC inclui dois grandes domínios tectônicos, o Domínio Rio Maria do Mesoarqueano no Sul e o Domínio Carajás (DC) do Neoarqueano no Norte (Vasquez et al. 2008; Fig. 2). O mais importante depósito de óxido de ferro– cobre e ouro (IOCG) é o depósito do Salobo de classe mundial que se encontra localizado no norte do DC, com reservas relatadas de 1,4 Gton a 0,82% de cobre e 0,49 g/t de ouro (VALE, 2012). Modelos propostos para a mineralização do Salobo o interpretaram como um depósito (IOCG) *"atípico"* devido ao seu minério incomum dominado por uma associação de magnetita-bornita-calcocita, por sua vez relacionado a clorita, actinolita, fluorita, calcita e hematita e quartzo em proporções menores (Lindenmayer and Teixeira, 1999; Melo et al., 2017; Vieira et al., 2019).

Modelos genéticos iniciais da mineralização do depósito de Salobo sugeriram que as rochas hospedeiras tinham uma origem sedimentar-vulcão exalativa submetida a um metamorfismo de médio a alto grau (Lindenmayer, 1990). Posteriormente Huhn Bacelar (1996), incluiu a mineralização de Salobo na classe de depósitos IOCG seguindo a proposta de Hitzman et al. (1992), com base nos procesos iniciais de albitização seguidos de alteração potássica, além da associação de minério com intrusões plutônicas felsicas de ~ 2.5 Ga. Adotando essa classificação, Requia et al. (2003), propuseram que a formação do depósito de Salobo resultou de uma intrusão de granito Old Salobo (2573 ± 2 Ma; Machado et al. (1991) com base nas idades Re-Os em molibdenita relacionada a sulfetos de cobre (2576 ± 8 e 2562 ± 8 Ma). Além disso, Melo et al. (2017) indicaram que o principal evento de mineralização do IOCG hospedado pelas rochas gnáissicas do Complexo Xingu (2.950 ± 25 e 2.857 ± 7 Ga) e granitoides da Suíte Igarapé Gelado (2.763 ± 4 Ga); provavelmente ocorreu ao mesmo tempo que a intrusão do Granito Old Salobo e a reativação da Zona de Cisalhamento Cinzento em torno de 2,5 Ga, porém apresenta uma evolução complexa com eventos hidrotermais sobrepostos, possivelmente com pulsos hidrotermais associados.

Por outro lado, Tassinari et al. (2003), consideraram uma origem hidrotermal para o minério, em torno de 2,7 Ga, a qual sofreu remobilização em estruturas rúpteis-dúcteis durante uma evolução policíclica da Zona de Cisalhamento Cinzento em ~ 2,5. Posteriormete, com base nas idades isocrônicas de Pb-Pb em Calcocita (2705 ± 42 Ma), Turmalina (2587 ± 150 Ma), Calcopirita (2427 ± 130 Ma) e Magnetita (2112 ± 12 Ma), Tassinari et al. (2003), indicou que a mineralização foi afetada por um metamorfismo de baixo grau e plutonismo granítico anorogênico em torno de 2,1 e 1,8 Ga, respectivamente.

Também nesse contexto, dados geocronológicos obtidos em rochas graníticas intrusivas e extrusivas na Província de Carajás (Requia et al. 2003; Tassinari et al. 2003; Vasquez et al. 2008; Feio et al. 2013; Melo et al. 2017; Pollard et al. 2018) apontam para dois grandes períodos de magmatismo granítico entre ~ 2,76 - 2,73 Ga e em torno de 1,88 Ga; assim, porém o significado dos diferentes eventos magmáticos e seu papel na origem e evolução da mineralização de depósitos de Salobo permanece controverso. Recentemente, em um estudo mineralógico-textural, Vieira et al., (2019), revisou a sequência paragenética e sugeriu um modelo evolutivo composto por várias etapas, que incluem i) a mineralização "primária" do tipo IOCG, relacionada a um magmatismo bimodal em ~ 2,75 - 2,74 Ga, seguido de ii) recristalização de magnetita por um metamorfismo de baixo grau, associado à reativação tectônica do sistema strike-slip de Carajás-Cinzento ~ 2,75 Ga; e iii) remobilização de sulfetos de Cu devido a uma pulso termo-hidrotermal relacionado ao magmatismo granítico anorogênico de idade Sideriano-Estateriano no Cráton Amazônico.

A partir das diferentes gerações de magnetita e a sequência paragenética proposta por Vieira et al., (2019), se escolheram amostras representativas dos principais estágios de magnetita para os análises geoquímicos: Alteração Ca-Fe "*brecha á magnetita* – Mgt tipo I" e a Mineralização de Cu-Au "*brecha á calcopirita* – Mgt tipo II", ambos formados por um evento magmático-hidrotermal; por último um metamorfismo deformacional sobreposto representado em "*xistos de magnetita* – Mgt tipo III". Os três tipos de magnetita apresentam padrões composicionais semelhantes, no entanto, ressaltassem algumas variações: A primeira magnetita (Mgt tipo I) é rica em Pb (média 884 ppm), enquanto a segunda (Mgt tipo II) presenta maiores concentrações de Cu (média 712 ppm), e a terceira (Mgt tipo III) contem altos valores de V (média 503 ppm) e Ti (média 1610 ppm).

A assinatura de isótopo de enxofre $\delta^{34}S$ foi determinada dos sulfetos de Cu-Fe (Pirita, Calcopirita e Pirrotita) presentes na brecha de calcopirita e em relação com a Mgt II Os dados isotópicos de enxofre em sulfetos de Cu-Fe do depósito IOCG Salobo, sugerem em conjunto com as associações texturais da calcopirita uma fonte de enxofre para a mineralização principalmente magmática sem/ou com contribuições mínimas de fluidos altamente salinos externos. Portanto, a desproporcionalização do enxofre desencadeada pela oxidação inicial da magnetita no fluido de caráter magmático-hidrotermal e evoluindo ao longo de caminhos químicos oxidados e reduzidos pode ser o processo chave para a geração da mineralização IOCG de Cu em Salobo.

Deste modo, este trabalho apresenta análises de elementos traços junto com relações texturais-minerais em magnetita do depósito IOCG Salobo, caracterizando as afinidades da magnetita entre os diferentes estágios de mineralização e a sequência paragenética anteriormente apresentada por Vieira et al., (2019); juntamente com dados de isótopo de enxofre de sulfetos de Cu-Fe do depósito IOCG Salobo. Em conjunto nossos resultados avaliam a aplicabilidade de diagramas propostos para a discriminação de magnetita e fornecem um arcabouço para elucidar os processos e possíveis mecanismos que levaram à formação e a evolução do minério do tipo IOCG em Salobo, levando em consideração processos propostos para sistemas magmático-hidrotermais de alta temperatura, no caso a "*crise da magnetita*" proposta por Jenner et al. (2010).

Manuscrito

To be submitted to Ore Geology Reviews

The giant metamorphosed IOCG Salobo deposit, Carajás Mineral Province: Magnetite trace elements and sulphides isotopic composition and implications for the metallogenetic model

Instituto de Geociências, Universidade de Brasília, Brasília – DF 70910-900, Brazil.

Highlights

- The Salobo **magnetite** was formed by magmatic-hydrothermal processes.
- The three generations of magnetite present **similar geochemical signature** since the proposed discrimination diagrams do not allow for a clear distinction in the chemical variation
- **S isotopes** corroborate an exclusive magmatic-derived sulfur source.
- Cu-Fe sulfides formation could have been driven by the **sulfur disproportionation** induced by magnetite crystallization.

Abstract

The genesis of IOCG deposits has been intensely debated, in particular, conceptual models are not yet clear whether the sulfur source is derived from the same magma source or have external contributions and which hydrothermal processes create the iron oxide enrichment. The Salobo deposit is a world-class iron oxide copper and gold (IOCG) deposit located in the Carajás Mineral Province, southeastern Amazon Craton, Brazil. It contains resources of 986 Mt @ 0.82% Cu and 0.49 g/t Au. The ore is characterized by a high tenor of copper-sulfides (bornite and chalcocite) hosted in magnetite-rich rocks with superimposed hydrothermal alteration and metamorphism-deformation, which have complicated ore-genesis and the geochemical interpretations. In this study, we combine mineralogical and chemical analysis of magnetite with sulfur isotopes on Cu-Fe sulfides of the Salobo deposit. Mineralogical studies show that there are three magnetite types including massive, pristine to inclusion-poor *magnetite breccia* (Mgt type I); inclusion-rich *magnetite-bearing breccia* (Mgt type II), and the granoblastic *magnetite schist* (Mgt type III). The Mgt type I is characterized by an association with high-temperature Fe-rich silicate minerals (i.e., ferrosilite, fayalite and hastingsite), whereas the Mgt type II is associated with Cu-Fe sulfides relate to chalcopyrite-rich breccias and the Mgt type III is related to schist with discordant veins of low-temperature Cu-Fe sulfides. In general, the trace element composition of these magnetites is similar without display a distinctive geochemical trend in discrimination diagrams. Thus, the Mgt type III represents recrystallization possible of the other magnetite types during Neoarchean metamorphism/metasomatism with an overprint of magmatic-hydrothermal alteration during the Paleoproterozoic. The range in $\delta^{34}S_{V\text{-}CDT}$ of 0.88 to 5.04‰ is consistent with a magmatic-hydrothermal sulfur source without/or minimal external contributions and indicates a sulfur disproportionation process in the early sulfide formation. Therefore, our data support that the magnetite types I and II were formed from an evolving oxidized-magmatic-hydrothermal Cu-rich fluid, under non-oxidizing atmospheric conditions. Moreover, the magnetite oxidation (crystallization) triggered the sulfur disproportionation, thus the sulfate reduction and the sulfide formation. Subsequent low-grade metamorphism associated with the emplacement of the Old Salobo Granite and reactivation of the Cinzento Shear Zone in ca. ~2.5 Ga resulted in the recrystallized Mgt type, which subsequently underwent hydrothermal alteration as a result of Paleoproterozoic magmatism.

Keywords: Iron oxide copper-gold, Sulfur isotopes, Magmatic-hydrothermal, Sulfur disproportionation.

1 Introduction

One of the most attractive Cu-Au deposits is the world-class iron oxide copper-gold (IOCG) ones, thanks to their higher contents of Cu and Au grades (Williams et al., 2005). Worldwide, the IOCG deposits have similar aspects of the geological environment and mineral association. These deposits generally are Fe oxide rich, present Na-Ca pre-sulfide alteration, show strong structural control and are formed by magmatic-hydrothermal fluids (Barton, 2014; Groves et al., 2010; Hitzman et al., 1992; Richards and Mumin, 2013; Williams et al., 2010, 2005). In general, these deposits are found in wide distribution in space and time, from post-orogenic settings from the late Archean (e.g., Carajás district, Brazil) and Proterozoic (e.g., Olympic Damn, Australia; Great Bear, Canada), to active continental margin of Andean Cordillera from Mesozoic (e.g., Candelaria and Punta del Cobre, Chile; Richards and Mumin, 2013; Sillitoe, 2003; Williams et al., 2005). Metamorphosed IOCG deposits present hydrothermal alteration-mineralization zoning textures preserved in deformed and metamorphosed belts with superimposed brittle-ductile deformation (e.g., Great Bear, Canada (Acosta-Góngora et al., 2018); Salobo, Brazil (Schutesky and Gouveia de Oliveira, *accepted.*; Vieira et al., 2019); Norrbotten, Sweden (Gleeson and Smith, 2009; Storey and Smith, 2017).

The world-class Salobo deposit, located in the Carajás Mineral Province in the southeastern part of the Amazonian Craton – Brazil, presents reported reserves of 1,4 Gton @ 0.82% Copper and 0.49 g/t Gold (VALE, 2012). Proposed models for the mineralization of the Salobo interpreted it as an atypical (IOCG) deposit with unusual ore mineralogy dominated by an association of magnetite – bornite – chalcocite, related with chlorite, actinolite, fluorite, calcite and minor hematite and quartz (Lindenmayer and Teixeira, 1999; Melo et al., 2017; Vieira et al., 2019). Based on a molybdenite Re-Os age of 2576 ± 8 and 2562 ± 8 Ma, Requia et al. (2003) linked the mineralization with the emplacement of the alkaline, metaluminous, syntectonic Old Salobo Granite (2573 ± 2 Ma; Machado et al. 1991). Conversely, Tassinari et al. (2003), interpreted the isochronic

chalcocite Pb-Pb age of 2705 ± 42 Ma as the timing of primary syngenetic origin for the mineralization with late remobilization stages in a polycyclic evolution, as a reactivation of the Carajás-Cinzento strike-slip system at ca. ~2.5 Ga.

In this context, geochronological data in the Carajás Province (Feio et al., 2013; Melo et al., 2017; Moreto et al., 2015; Pollard et al., 2018; Requia et al., 2003; Tassinari et al., 2003; Vasquez et al., 2008) and further paragenetic-mineralogical study (Vieira et al., 2019) reviewed the paragenetic sequence and suggested a multi-stage evolutionary model for the Salobo deposit, which included i) the "primary" IOCG-type mineralization, related to bimodal magmatism at ca. ~2.75 - 2.74 Ga, followed by ii) magnetite-recrystallization at low-grade metamorphism, associated with the tectonic reactivation of the Carajás-Cinzento strike-slip; and iii) Cu-remobilization due to a thermal-hydrothermal imprint related with the emplacement of Siderian-Statherian anorogenic granitic magmatism in the Amazonian Craton.

Conceptual models on IOCG formation (Barton, 2014; Chen, 2013; Pollard, 2006; Williams et al., 2010, 2005) that involve magmatic sulfur source (Acosta-Góngora et al., 2018; Pollard, 2006; Schlegel et al., 2017) suggests that iron oxides associated with Cu-Fe reflect sulfur-poor mineralization that typically needs an oxidized sulfur source rich in sulfate (Barton, 2014; Hitzman et al., 1992; Richards and Mumin, 2013; Williams et al., 2005). The reduction of sulfur is of critical importance for the Cu-sulfide ore precipitation (Barton, 2014; Williams et al., 2005), which can be generated by the reduction of sulfate (e.g., Barton 2014), by sulfur remobilization from pre-existing sulphides such as pyrite (Schlegel et al. 2017, and references therein) and by addition of sulfur from an external fluid (e.g., Chen 2013). It has been proposed that the key process for the sulfate reduction in oxidized magmas is the magnetite crystallization which entails ferrous iron oxidation (Sun et al., 2015, 2013), playing a significant role for the sulfide saturation in a melt (Jenner et al., 2010).

Magnetite has a general stoichiometry AB_2O_4 in an inverse spinel structure (Biagioni and Pasero, 2014), where trace elements (e.g., Mg, Ni, Mn, Co, Zn, Al, Cr, V, Mn, Cu, Ge, Ga; Nadoll et al. 2014 and references therein) can be incorporated by substitution with Fe^{3+} and Fe^{2+} in tetrahedral or octahedral sites (Dupuis and Beaudoin, 2011; Huang and Beaudoin, 2019; Nadoll et al., 2014). The compositional variability of magnetite reflects formation conditions and the composition of magma or hydrothermal solutions

(Dare et al., 2014; Nadoll et al., 2014), thus, magnetite has been proposed as a petrogenetic indicator and pathfinder for iron-oxides deposit types using discriminant diagrams (Dare et al., 2014; Dupuis and Beaudoin, 2011; Knipping et al., 2015; Nadoll et al., 2014; Wang et al., 2018). Besides, processes of recrystallization, dissolution and reprecipitation can be recorded in both magnetite textures and t trace element composition (Wen et al. 2017; Huang and Beaudoin 2019, among others). Therefore, textural and chemical analyses of magnetite are thus crucial to reveal and discriminate compositional trends helping to understand the magnetite evolution and formation processes for the Salobo deposit.

In this paper, we present compositional data linked to textural-mineral relationships for magnetite together with sulfur isotope analyses of Cu-Fe sulphides from the IOCG Salobo deposit. This study evaluates the applicability of current magnetite discrimination plots and characterizes the different textural occurrences of magnetite to elucidate the processes and possible mechanism involved in the ore formation, providing insights for IOCG ore formation involving processes similar to those proposed for high-temperature magmatic-hydrothermal systems such as the "*magnetite crisis*" (Jenner et al., 2010).

2 Geological Background

The Carajás Mineral Province (CMP) is located in the Pará state, northern Brazil, and constitutes the oldest crustal segment of the Amazonian Craton (Vasquez et al. 2008). The CMP includes two major tectonic domains, namely the Mesoarchean Rio Maria Domain in the south and the Neoarchean Carajás Domain (CD) in the north (Fig.1A) (Vasquez et al. 2008). All known Iron oxide-copper-gold (IOCG) deposits are located in the CD, the most important is the world-class Salobo deposit in the north with reported reserves of 986 Mt @ 0.82% Cu and 0.49 g/t Au (Xavier et al., 2012).

The Carajás Domain consists of Mesoarchean basement and Neoarchean intrusive and supracrustal units (Machado et al., 1991). Basement rocks include granites, tonalitic to granodioritic polymetamorphic orthogneisses and migmatites of the Xingu Complex in amphibolite and granulite facies (2974 ± 15 Ma, Pb-Pb zircon, Avelar et al. 1999; 3066

± 6,6 Ma, U-Pb zircon, Delinardo da Silva 2014) and mafic granulites of the Pium Complex or Chicrim-Cateté Orthogranulite (3002 ± 14 Ma, U-Pb zircon; Pidgeon et al. 2000). Geochronological data of migmatization (2859 ± 2 Ma and 2860 ± 2 Ma, U-Pb zircon; Machado et al. 1991) and granulitization (2859 ± 9 ma, U-Pb zircon, Pidgeon et al. 2000) of the Xingu Complex suggests that these processes could have been contemporaneous.

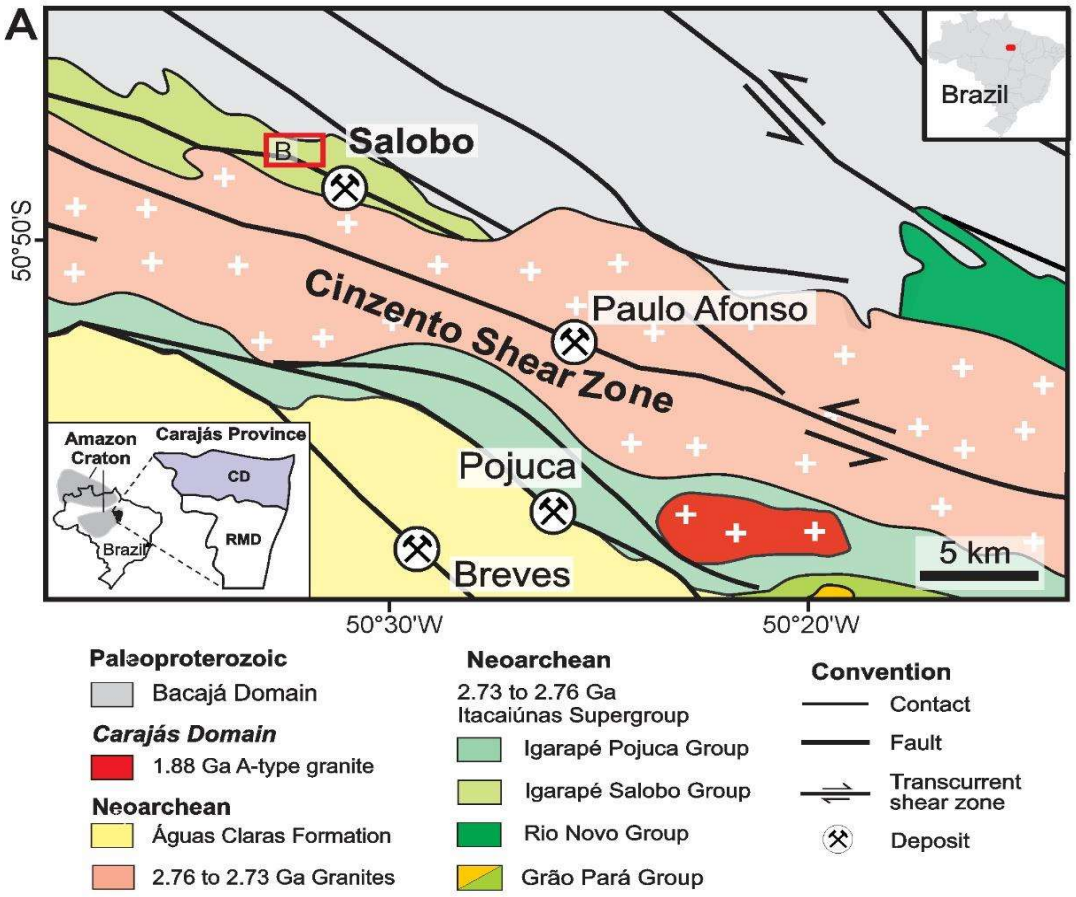

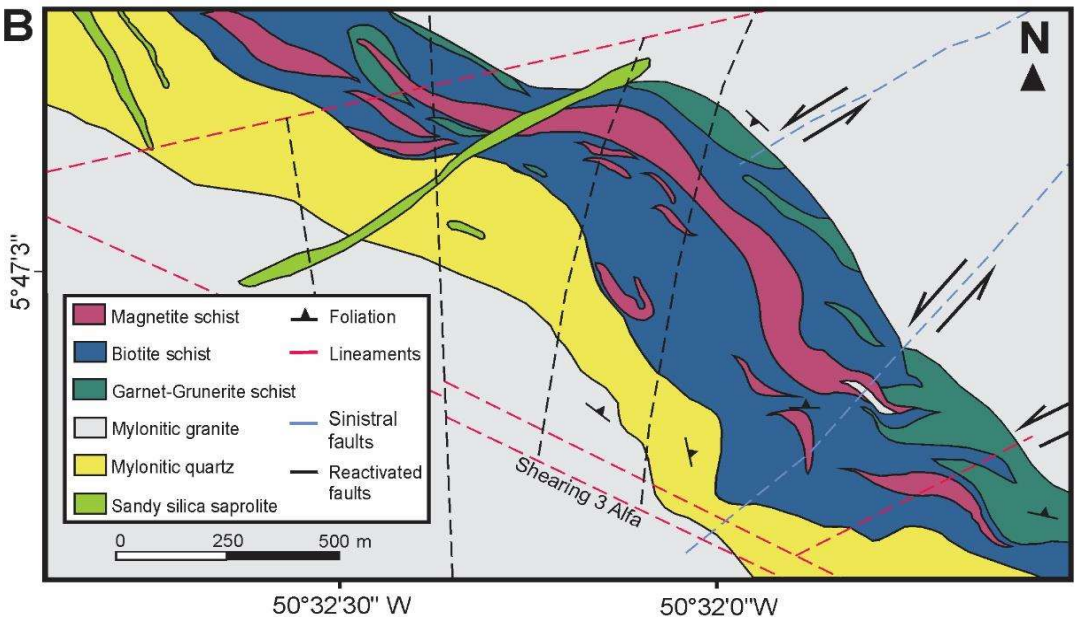

Fig. 1. (A) Simplified geological map of a part of the north of the Carajás Domain with the location of the IOCG Salobo deposit and the main shear zone (Modified from Melo et al. 2019). (B) Simplified geological map of the Salobo mine.

Metavolcano–sedimentary rocks of the Rio Novo Group and Itacaiúnas Supergroup rest unconformably on the basement rocks (Machado et al., 1991). Metamorphic rocks of low grade (mostly greenschist facies) as metaquartzites, metagreywacke and schists, and tholeiitic metavolcanic rocks and gabbros constituting the Rio Novo Group (2763 ± 7 Ma; Machado et al. 1991; Vasquez et al. 2008). The Itacaiúnas Supergroup is divided into four groups, all formed in an intracratonic basin between 2.76 and 2.73 Ga (DOCEGEO, 1988; Machado et al., 1991): (i) Igarapé Salobo includes gneisses, amphibolites, quartzites, metagreywackes and iron formations (Machado et al., 1991); (ii) Igarapé Pojuca, constituted of metasedimentary and metavolcanic rocks in greenschists to amphibolite facies; (iii) Grão Pará, composed of metabasalts, felsic metavolcanic rocks and jaspilites, which host giant iron deposits; and (iv) Igarapé Bahia, which contains metavolcanic, meta-pyroclastic and metasedimentary rocks (DOCEGEO, 1988; Machado et al., 1991). Subsequently, these sequences were affected by low-temperature metamorphism and hydrothermal alteration (Machado et al., 1991).

The Águas Claras Formation covers the Itacaiúnas Supergroup and is composed of a non-metamorphosed sequence of sedimentary rocks, deposited in a regressive environment from fluvial to shallow marine platform, such as meta-arenites, metapelites and meta–conglomerates (Pinheiro and Holdsworth 2000, and references therein). Ultramafic and mafic igneous intrusions crosscut the basement rocks and supracrustal sequences, and are represented by the ca. 2.76 ± 6 Ga Luanga Complex (Machado et al., 1991). These mafic-ultramafic layered complexes represent a major magmatic event coeval with the extensive felsic volcanism of the Grão Pará Group and are associated with chrome mineralization (Machado et al., 1991). The basin inversion in the Carajás Domain has been attributed to the deformation along the major NW-trending fault systems caused by the principal faults, namely the Cinzento and Carajás shear zones, which were active during periods since the Mesoarchean (Pinheiro and Holdsworth, 2000; Pollard, 2006) and underwent crustal extension at ca. 1.88 Ga (Tassinari et al., 2003).

The magmatic evolution related to the Salobo deposit in the Carajás Domain can be compressed in four principal events: Mesoarchean rock formation ~ 3.0 Ga of the

Tonalitic Gneisses of the Xingú Complex (Avelar et al., 1999; Delinardo da Silva, 2014); Neoarchean volcanism and deposition of the metavolcanic–sedimentary sequences of Salobo, Pojuca and Grão Pará groups at ca. ~ 2.8 - 2.7 Ga, together with the development of the primary copper mineralization, followed by high–medium metamorphic events (Tassinari et al., 2003); some re-equilibration and ore remobilization at ca. ~ 2.57 Ga related to the emplacement of peralkaline to metaluminous granitoids, which are represented by granitic bodies, such as Old Salobo and Itacaiúnas granites associated with the tectonic reactivation of Carajás Cinzento Shear Zone (Machado et al., 1991; Tassinari et al., 2003); Paleoproterozoic ca. ~2.1 Ga hydrothermal alteration associated with low-grade metamorphism (Tassinari et al., 2003) and ca. ~1.88 Ga alkaline to sub–alkaline A-type granites, possibly related to the Transamazonian Orogeny (e.g., Young Salobo and Cigano granites; Machado et al. 1991; Lindenmayer and Teixeira 1999).

The main ore minerals of Salobo deposit are bornite, chalcocite and digenite associated with high-grade magnetite schist, accompanied by an intensive hydrothermal alteration related to mylonitic rocks with varying amounts of almandine, chlorite and feldspar sericitization (Lindenmayer, 1990; Lindenmayer and Teixeira, 1999). This is overprinted by breccia, veins and replacement-style that includes chalcopyrite, molybdenite, uraninite, graphite, pentlandite, pyrite, covellite and hematite, and a variety of minor phases, like fluorite, apatite and zircon (Vieira et al., 2019). Salobo is located close to the Cinzento Shear Zone, which activity resulted in intense metamorphism-deformation and pervasive hydrothermal alteration overprints the Salobo deposit (Melo et al., 2017) generating several interpretations for the type of deposit for the Salobo ore (Lindenmayer, 1990; Machado et al., 1991; Melo et al., 2019, 2017; Requia et al., 2003; Tassinari et al., 2003; Tavares et al., 2018; Vieira et al., 2019; Xavier et al., 2012).

At first, the host rocks were thought to be iron formations of a VMS deposit that underwent high-grade metamorphism (Lindenmayer, 1990), then Huhn Bacelar, (1996) included the Salobo mineralization in the IOCG deposit class based on early albitization processes followed by potassic alteration, besides the ore association with plutonic felsic intrusions of 2.5 Ga. In this perspective, Requia et al. (2003) proposed that the deposit formation resulted from a granite intrusion based on the Re-Os ages in molybdenite related to copper sulfides (2576 ± 8 Ma), which is coherent with the Old Salobo Granite age; and Melo et al. (2017) indicated that the main IOCG mineralization event probably occurred at the same time as the Old Salobo Granite at around 2.5 Ga, which presents a

complex evolution with superimposed hydrothermal events and is hosted by the gneissic rocks of the Xingu Complex (2.950 ± 25 and 2.857 ± 7 Ga) and granitoids of the Igarapé Gelado Suite (2.763 ± 4 Ga). In contrast, Tassinari et al. (2003) considered a hydrothermal origin for the ore around 2.7 Ga, which suffered later remobilization and metamorphic events, based on Pb-Pb ages in chalcocite (2705 ± 42 Ma), tourmaline (2587 ± 150 Ma), chalcopyrite (2427 ±130 Ma) and magnetite (2112 ± 12 Ma).

3 Material and Methods

The mineral assemblage and textural relationships between ore and gangue minerals were investigated in 24 polished thin sections by transmitted and reflected light microscopy. Magnetite spot analyses and compositional maps of major and minor elements were obtained using a 5-spectrometer JEOL JXA-8230 SuperProbe at the Electron Microprobe Laboratory of the University of Brasília (Brazil). A total of 24 elements were measured (i.e., Si, Ca, Y, P, Pb, Zr, Hf, Al, Ge, W, Ta, Nb, Cu, Mo, Sn, Ga, Mn, Mg, Ti, Zn, Co, V, Ni, and Cr), from which Fe, V, Ti, Mg, Si, Cu were selected for the compositional maps. The wavelength dispersive (WDS) analyses were performed at an accelerating voltage of 15 kV and a beam current of 10 nA. Both synthetic and natural mineral standards were used for the analyses and the same standards and procedure were retained throughout the analytical work. Systematic WDS analyses were obtained for magnetite. Oxygen content is calculated based on the ideal formula (Droop, 1987).

Multiple S isotopes (^{32}S, ^{33}S, and ^{34}S) were determinate for Cu-Fe sulphides associated with magnetite, using a Cameca IMS1270 instrument located at the Swedish Museum of Natural History, Stockholm (NordSIMS facility). Analytical methods and instrument parameters followed are those described by Whitehouse et al. (2005). In a brief description, a primary beam with an incident energy of +10 kV, illumination of ca. 100 µm resulted in a typical beam current of ca. 10 – 20 nA and produced an elliptical, flat-bottomed shaped crater. The mass spectrometer was operated with a high mass resolution ($M / \Delta M \approx 8000$). Normal incidence electron flooding gun for charge compensation, – 10 kV secondary beam, software (Cameca CIPS, version 4) automated centring of the entrance slit, field aperture, and mass, with simultaneous detection of three

Faraday cup detectors positioned along the focal plane for simultaneous measurement of ^{32}S, ^{33}S and ^{34}S, operated at an effective high mass resolution of ca. 4600 on the ^{33}S channel.

4 Results

We have studied a suite of representative samples types from the pressure shadow zone of the Salobo mega sigmoid (Fig. 1B); which include granitic rocks with hydrothermal alteration (Fig. 2A), magnetite (Fig. 2C) and chalcopyrite hydrothermal breccia (Fig. 2D), garnet-biotite and magnetite-rich schists (Fig. 2E). These rocks are exposed in meter-scale, low-strain sigmoidal domains (Q-domains), within the mylonitic fabric, and transitionally grades towards the schists.

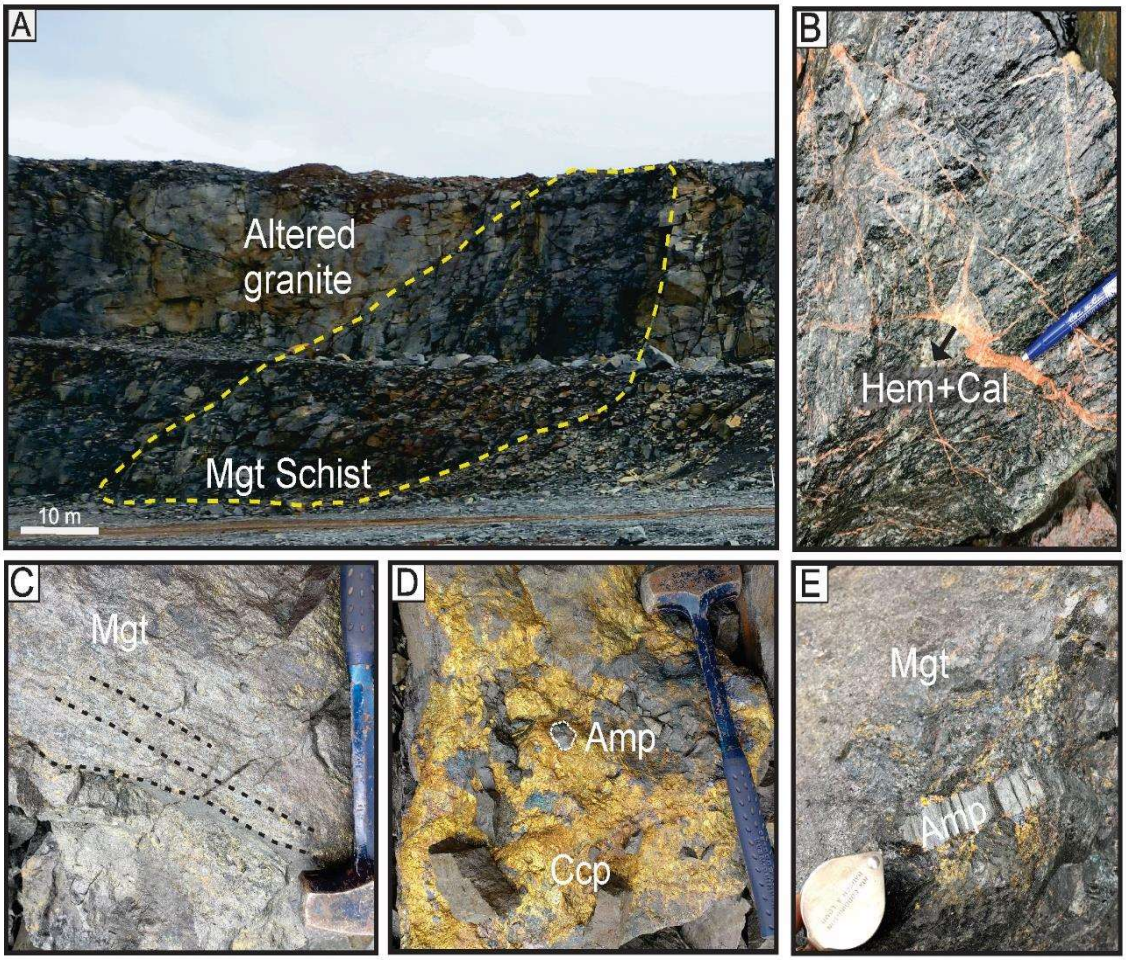

Fig. 2. A. Section through the giant Salobo mining area showing the domains of the magnetite-rich schist rocks related to the granitic rocks with hydrothermal alteration. Macroscopic ore

samples: B. Hemtatite+Calcite veins cross-cutting the foliation of the magnetite-rich schist. C. Magnetite-rich schist with orientated chalcopyrite. D. Matrix supported hydrothermal chalcopyrite breccia with magnetite and amphibole clasts. E. Magnetite breccia with amphibole grains surrounded by chalcopyrite. Amp: amphibole. Cal: Calcite. Ccp: Chalcopyrite. Hem: hematite. Mgt: Magnetite.

The Cinzento Shear Zone influence affects the host rock of the deposit through vertical corridors of transcurrent faults, as a result, the hydrothermally altered granitic rocks that host the mineralization are cut vertically by the magnetite-rich schist (Fig. 2A) at the inner part and by garnet-biotite schist at the edges. Along these corridors, lenses of magnetite-bearing chalcopyrite breccia were preserved (Fig. 2D). The host and wall rocks in the Salobo mine are strongly folded and deformed in addition to presenting an intense and pervasive hydrothermal alteration, thus is not possible to distinguish a clear zonation of the hydrothermal alterations.

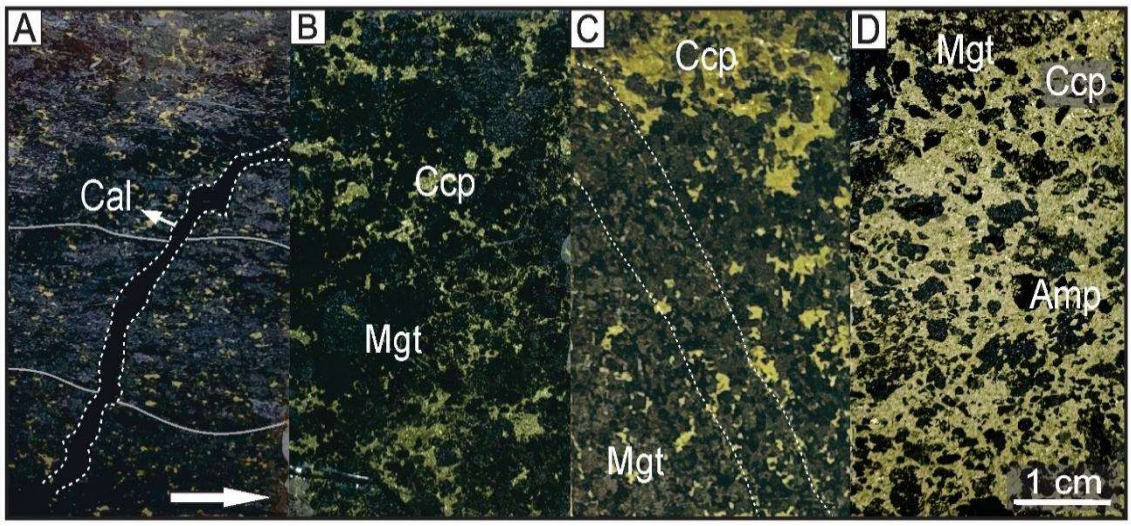

Fig. 3. Photos of thin sections showing a gradual change in the matrix composition of the hydrothermal breccias from more deformed magnetite-matrix (B) to fresh massive chalcopyrite-matrix (D). A. Magnetite-rich schist with interstitial chalcopyrite grains and a discordant vein of calcite. B. Matrix supported magnetite breccia with chalcopyrite. D. Chalcopyrite breccia with subhedral magnetite and amphiboles grains. Amp: amphibole. Cal: Calcite. Ccp: Chalcopyrite. Mgt: Magnetite.

The textural and mineral relationships of the magnetite from the representative samples of the Salobo deposit allowed to distinguish different textural magnetite types (Table 1), which crop out in the pressure shadow zone of the Salobo mega sigmoid (Fig. 1B). The textures comprise massive and granular pristine to inclusion-rich magnetite

grains (Fig. 4). Granitic rocks with hydrothermal alteration and garnet-biotite schists contain only minor amounts of ore, while the higher-grade ore belongs to magnetite-rich schist and hydrothermal amphibole-bearing breccia with chalcopyrite matrix Vieira et al., (2019).

Table 1

Summary information of magnetite types from the IOCG Salobo deposit.

Magnetite Type	Magnetite textures	Important Associated minerals		Magnetite inclusions	Host Rocks
		Metallic	Gangue		
Type I	Massive Granular	Ccp, Bn grains-veins	Hst, Fs, Fa	Mnz, Ap	Mgt breccia
Type II	Granular	Py, Po, Pn	Act, Amp, Chl	Mnz, Zrn, Urn, Ap, Ccp, Bn, Py	Ccp breccia
Type III	Granoblastic	Hem, Bn, Cv, Cct, Dg veins Mol, Gr, Ilm	Fl, Cal, veins Bt, Qz, Chl, Grt	Inclusion-poor	Mgt-rich schist

Note: Mineral abbreviations= Act: actinolite, Amp: amphibole, Ap: apatite, Bn: bornite, Bt: biotite, Cal: calcite, Ccp: chalcopyrite, Cct: chalcocite, Chl: chlorite, Cv: covellite, Dg: digenite, Fa: fayalite, Fs: ferrosilite, Fl: fluorite, Gr: graphite, Grt: garnet, Hst: hastingsite, Hem: hematite, Ilm: ilmenite, Mgt: magnetite, Mnz: monazite, Mol: molybdenite, Pn: pentlandite, Po: pyrrhotite, Py: pyrite, Qz: quartz, Urn: uraninite, Zrn: zircon.

Magnetite-breccia (Mgt type I)

The Mgt type I is related to a magnetite-breccia with a supported matrix of coarse-grained magnetite in a massive texture (Mgt type I; Fig. 3B), which cements an association of iron-rich silicates such as ferrosilite, fayalite and hastingsite (Fig. 4A) Some grains of fayalite and ferrosilite are altered to chlorite. Interstitial grains and veins of chalcopyrite and bornite grains are also present close to the iron-rich silicates, both not bigger than ~80µm (Fig. 4B). The coarse-grained Mgt type I is inclusion-poor with some monazite and apatite visible grains as inclusions. Some magnetite grains exhibit veins and borders of actinolite (Fig. 4C).

Chalcopyrite-breccia (Mgt type II)

A gradual change in the amount of the matrix composition from magnetite to chalcopyrite resulted in a chalcopyrite-breccia that contents the Mgt type II (Fig. 3). The Mgt type II is characterized by larger grains (~0,3mm – 8mm) isolated in the chalcopyrite matrix (Fig. 3D), which also hosts a distribution of sulphurs, such as pyrite, pyrrhotite, pentlandite and siegenite (Fig. 4E, F). Some pyrite grains show chalcopyrite replacement (Fig. 4E) and pyrrhotite exsolutions (Fig. 4F). Magnetite type I grains and Fe-rich mineral/fragments of amphibole are present close to the inclusion-rich Mgt type II with fuzzy (Fig. 4C) to regular (Fig. 5) boundaries. The inclusions of this magnetite are randomly distributed varying from 3µm – 60 µm approximately and are composed by REE- monazite, zircon, uraninite, apatite and Cu-Fe sulfides, namely, pyrite, bornite and chalcopyrite (Fig. 4D, 5). The inclusions grains of apatite were identified by EPMA as fluorapatite with F content of 2,04 – 4,56 wt ‰ and average Cl content of 0,05 wt ‰. It is a minor mineral phase compared to Cu-Fe sulphides and is present as disseminated subhedral grains.

Magnetite schist (Mgt type III)

Finally, the Mgt type III magnetite is related to magnetite schists which host the ore association of bornite-chalcocite-digenite and magnetite. The schist present minor bands of biotite and recrystallized quartz that involves garnets with sigmoidal pressure shadows. The orientation of magnetite grains that follows the schist foliation is the principal feature of the equigranular, granoblastic and inclusion poor (non-visible at petrographic scale) Mgt type III (Fig. 4G). The chalcopyrite related to the Mgt type III appears as veins that also follows the schist foliation (Fig. 2C). The magnetite type III grains are not bigger than 100 µm and their boundaries are predominantly regular and sharp in contact with other magnetite and ilmenite grains. Some magnetite grains show well-defined 120°tiple junctions (Fig. 4G). The Mgt type III is also associated with coarse-grained garnet (i.e., almandine) which surrounds some magnetite grains. Ilmenite exsolutions are only present in porphyroblasts of magnetite (>100 µm – 700 µm; Fig. 3G). Bornite is present as grains with exsolutions textures of chalcocite, digenite and covellite and as discordant veins

together with digenite, chalcocite, covellite, fluorite, calcite and hematite (Figures 2B, 3A, 4H, I), which are cutting the magnetite foliation with some associated graphite. Fibrous and deformed molybdenite with undulant extinction is also present (Fig. 4I).

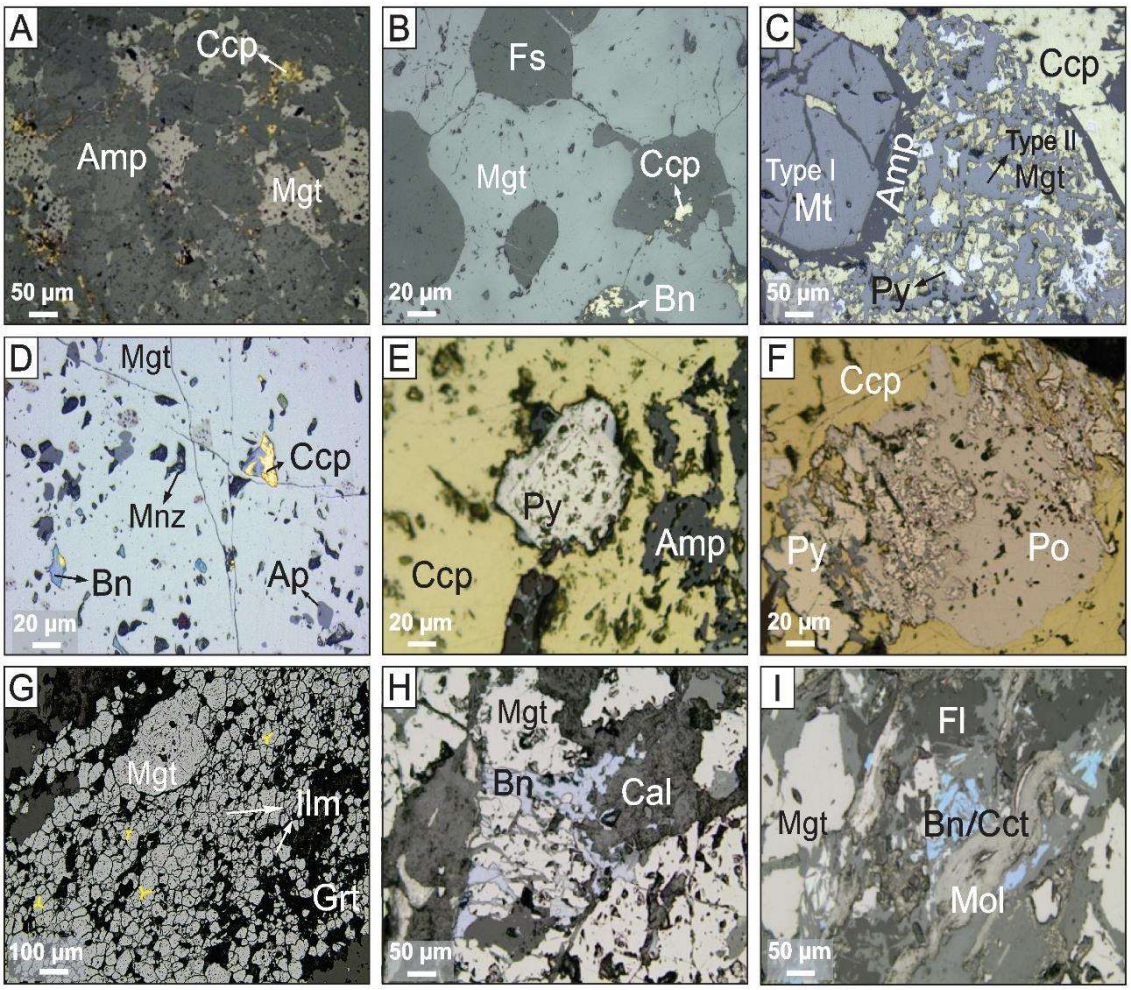

Fig. 4. Micro-photographs of representative thin sections showing textures of the *magnetite breccia* – Mgt type I (A, B), the *chalcopyrite breccia* – Mgt type II (C, D, E, F) and the *magnetite schist* – Mgt type III (G, H, I). (A) Massive magnetite associated with amphibole and disseminated chalcopyrite. (B) Pristine-massive magnetite associated with ferrosilite. (C) Magnetite grain (Mgt type I) close to amphibole and pyrite-chalcopyrite assemblage in pre-existing magnetite (Mgt type II). (D) Magnetite with bornite, chalcopyrite, monazite and apatite inclusions. (E) Massive chalcopyrite with subhedral pyrite grain showing an alteration rim. (F) Pyrite crystal transforming to pyrrhotite in a chalcopyrite matrix. (G) Granular magnetite related to garnet with ilmenite exsolutions. (H) Granular-massive magnetite associated with calcite and bornite veins. (I) Fibrous oriented and deformed molybdenite associated with magnetite, fluorite and bornite with a lower-temperature phase of chalcocite. Mineral abbreviations: Amp: Amphibole. Ap: Apatite. Bn: Bornite. Cal: Calcite. Cct: Chalcocite. Ccp: Chalcopyrite. Fs: Ferrosilite. Fl: Fluorite. Grt: Garnet. Ilm: Ilmenite. Mgt: Magnetite. Mnz: Monazite. Mol: Molybdenite. Py: Pyrite. Po: Pyrrhotite.

4.1 *Trace elements in magnetite*

The elements average content of magnetite is presented in percentage (%) in table 2. The FeO content of magnetite for the three magnetite types is slightly higher, ranging from 77.53 and 93.88 wt% (consistent with magnetite stoichiometry, Dare et al., 2014). In general, the trace elements concentration for the three magnetite types is similar without lithogeochemical zonation.

The EPMA maps of the Salobo magnetite grains (Fig. 5) shows that Mgt Type II is very homogeneous and do not show any compositional zoning ore compositional trends in binary diagrams (Fig. 8), in which the Mgt type I, II and type III shows similar Si-Mg and Co-Cr concentrations (Fig. 8A, C), despite some higher correlation between Si and Mg of the Mgt type I (Fig. 8A). Besides, the Mgt type III shows higher V concentrations compared to the other magnetite types (Fig. 8D).

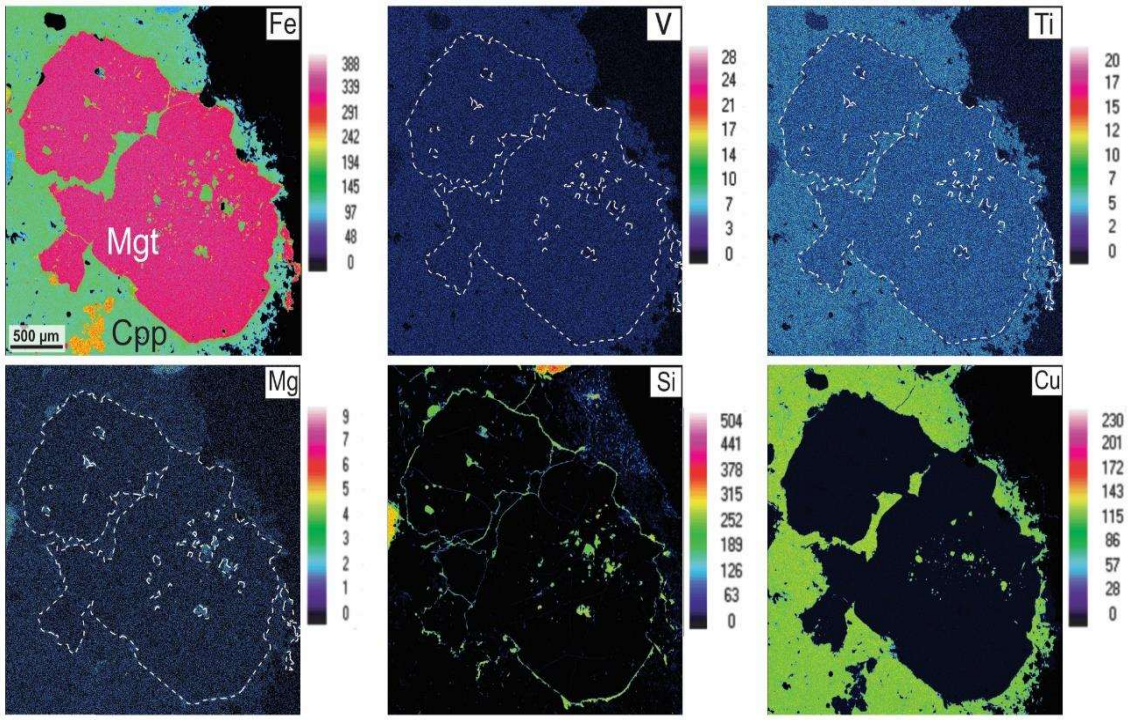

Fig. 5. Elemental WDS maps for a representative sample from *chalcopyrite breccia* – Mgt type II. Note the low Ti, V and Mg concentration in inclusion-rich magnetite. In general, the distribution of the element's content is very homogeneous. Colour bars indicate element concentration in wt‰. Ccp: chalcopyrite. Mgt: magnetite.

Table 2 - Representative trace element concentrations for magnetite occurrences (Mgt type I, II and type III) based on EMPA analyses. The corresponding graphics are shown in Fig. 6, 7.

	Type I			Type II			Type III		
Element	Ave	Min	Max	Ave	Min	Max	Ave	Min	Max
FeO	90,63	77,53	93,88	92,66	90,57	93,80	90,90	86,22	93,76
SiO_2	0,121	0,032	0,241	0,140	0,032	0,282	0,132	0,087	0,198
Al_2O_3	0,238	0,014	0,565	0,209	0,001	0,489	0,304	0,097	0,000
CaO	0,023	0,001	0,110	0,028	0,005	0,118	0,014	0,006	0,034
P_2O5	0,030	0,004	0,100	0,024	0,002	0,056	0,039	0,006	0,093
NiO	0,024	0,004	0,060	0,043	0,020	0,078	0,039	0,015	0,072
MnO	0,053	0,001	0,164	0,076	0,018	0,130	0,071	0,008	0,119
MgO	0,022	0,003	0,064	0,021	0,001	0,052	0,020	0,005	0,049
TiO_2	0,197	0,004	0,600	0,156	0,007	0,325	0,269	0,021	0,587
V_2O_3	0,049	0,001	0,194	0,026	0,005	0,019	0,090	0,011	0,196
Cr_2O_3	0,050	0,008	0,113	0,062	0,015	0,111	0,065	0,010	0,140
CoO	0,035	0,001	0,091	0,054	0,005	0,136	0,060	0,018	0,163
CuO	0,077	0,006	0,228	0,089	0,020	0,205	0,070	0,013	0,144
ZnO	3,742	0,682	7,927	3,894	0,082	7,855	3,313	2,071	6,650
MoO_3	0,069	0,001	0,238	0,075	0,003	0,198	0,053	0,013	0,118
PbO	0,095	0,002	0,256	0,063	0,016	0,159	0,070	0,033	0,119
ZrO_2	0,064	0,014	0,142	0,073	0,003	0,196	0,044	0,039	0,054
HfO_2	0,162	0,046	0,336	0,128	0,018	0,291	0,138	0,018	0,256
Y_2O_3	0,069	0,007	0,196	0,061	0,009	0,122	0,074	0,038	0,103
Ta_2O_5	0,122	0,015	0,321	0,101	0,002	0,176	0,117	0,003	0,251
Nb_2O_5	0,058	0,009	0,157	0,056	0,009	0,148	0,039	0,018	0,084
Ga_2O_3	BDL	BDL	BDL	BDL	BDL	BDL	0,020	0,016	0,027
GeO_2	0,681	0,140	1,260	0,493	0,281	0,845	0,530	0,141	0,706
WO_3	0,077	0,003	0,338	0,084	0,008	0,341	0,048	0,005	0,133
SnO_2	0,557	0,060	1,951	0,659	0,021	1,530	0,789	0,359	1,382
Sc_2O_3	BDL	BDL	BDL	BDL	BDL	BDL	BDL	BDL	BDL

Note: All concentrations reported in wt‰. Detection limits for all elements are 0.001 wt‰. BDL: Below detection limit.

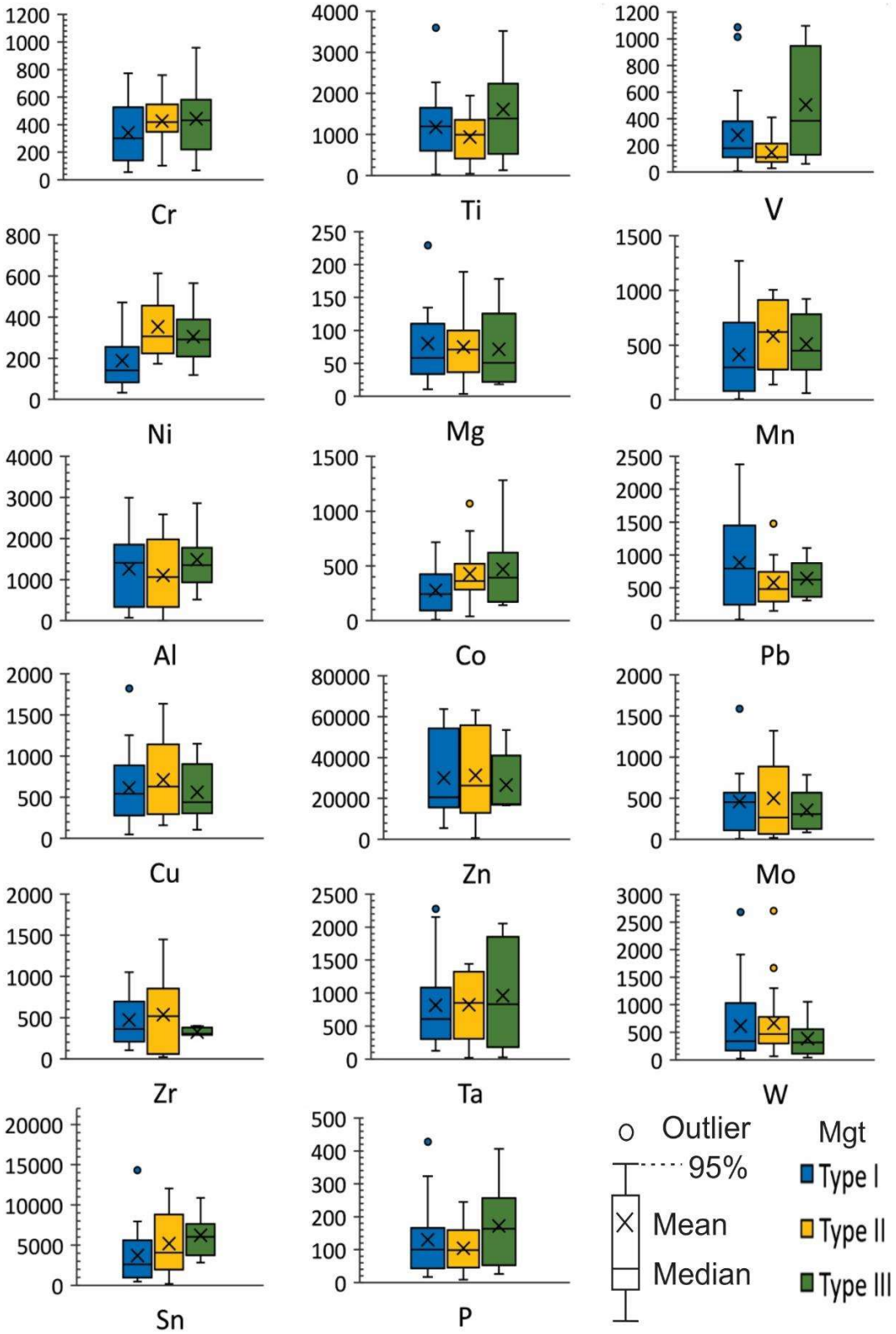

Fig. 6. Data distribution in ppm for important minor and trace elements variations of the magnetite types (Mgt type I, II and type III) in box and whisker plots. The upper and lower margins of the box represent the upper and lower 50 percentile of the data. The whiskers represent the upper and lower threshold values (95 percentile of the data). Mean values are shown as "*x*" and median values as solid black lines. See text for further discussion.

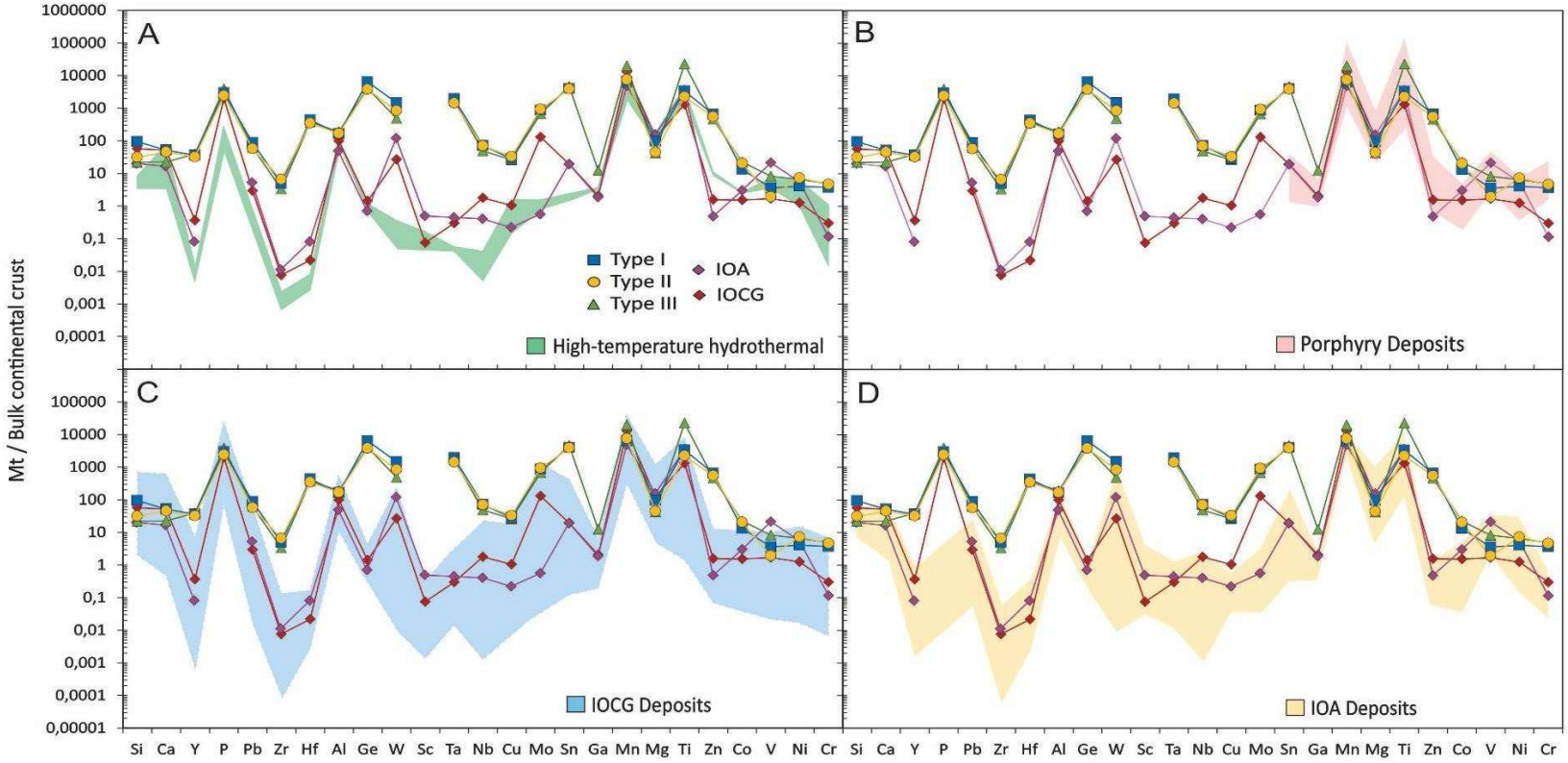

Fig. 7. Trace element EPMA results of magnetite grains from the three magnetite textures-types (Mgt type I, II and type III) at Salobo deposit plotted in a multielement variation diagram proposed by Dare et al, (2014) normalized to bulk continental crust (Rudnick and Gao, 2003). To achieve the original composition the results of this study include small exsolutions and inclusions following Dare et al., (2014). Values are compared to compilated compositional ranges of magnetite from high-temperature (>500°C) magmatic-hydrothermal (A. *green* from Dare et al., 2014) porphyry deposits (B. *pink* from Nadoll et al., 2014),. The average values of IOCG and IOA deposits, as well as its fields (C. IOCG – *blue* and D. IOA – *yellow*) from Huang et al., (2019).

The data were plotted in a box and whisker diagrams where is possible to easily visualize outliers of the breadth of the data group, thus it can be observed some outstanding variations (Fig. 6). Mgt type I and II shares similar concentration in Ti, Mg, Al, Cu, Zn and P, however, the Mgt type I which is associated with the Fe-rich silicates stand out for having higher concentrations of W (average 613 ppm W), Pb (average 884 ppm Pb) and Ni-poor (average 188 ppm N; Fig. 7B). The Cu values of the Mgt type II varying between 160 – 1638 ppm of copper, besides, the Mgt type II shows a slight enrichment in Ni, Mn, Mo and Zr concentration (ppm average 339 Ni; Fig. 7B, 585 Mn, 499 Mo and 537 Zr) and contains the lowest V values (average 146 ppm; Fig. 8D). The Mgt type III where ilmenite exsolutions in magnetite were observed, is the more depleted in Zr (average 325 ppm Zr), in contrast, is the more enriched in Ti, Ta and P (ppm average 1610 Ti, 959 Ta and 171 P) and present anomalous V concentration with ranges between 61 – 1098 ppm V when compared to the others magnetite types (Fig. 8D). The Cu concentration of the Mgt type III (ppm average 560 Cu; Fig. 6) shows similar values with the Mgt I and II types.

Additionally, the magnetite data were normalized to the bulk continental crust (data from Rudnick and Gao, 2003) in a multielement variation diagram (Fig. 7) proposed by Dare et al. (2014), in which 25 trace elements concentration are plotted in order of increasing compatibility into magnetite (Dare et al., 2014). Data is compared to high-temperature hydrothermal (>500ºC) magnetite defined from analytical results of different IOCG deposits (Dare et al., 2014; *green area*; Fig. 7A); and data for igneous and hydrothermal porphyry magnetite (Nadoll et al., 2014; *pink area*; Fig. 7B). The data source for IOA and IOCG fields (*orange and blue areas* respectively; Fig. 7C, D) and its average concentration from representative deposits are from Huang et al., (2019).

In general, trace elements patterns for the three magnetite types present a similar distribution (Fig. 7). Ga, Mn, Ti, V, Ni and Cr elements contents show a correlation with the fields of porphyry and the high-temperature magmatic-hydrothermal (>500°C) fields, which in turn present an overlapping with the IOCG as well as the IOA zone for the same elements. Moreover, it should be noted that V concentrations are significantly higher for IOA deposits, and Si, Ca, P, Pb, Al, Mo are in agreement with the IOCG field (Fig. 7C). Besides, the Si, Mn, Mg, Al, Ti and Ca concentrations in the magnetite are similar to the data from Huang et al., (2019) for the Salobo deposit, however, the chemistry results obtained in this study are noteworthy highly enriched in lithophiles elements, such as Ge,

W, Y, Zr, Hf and Ta (Fig. 7).

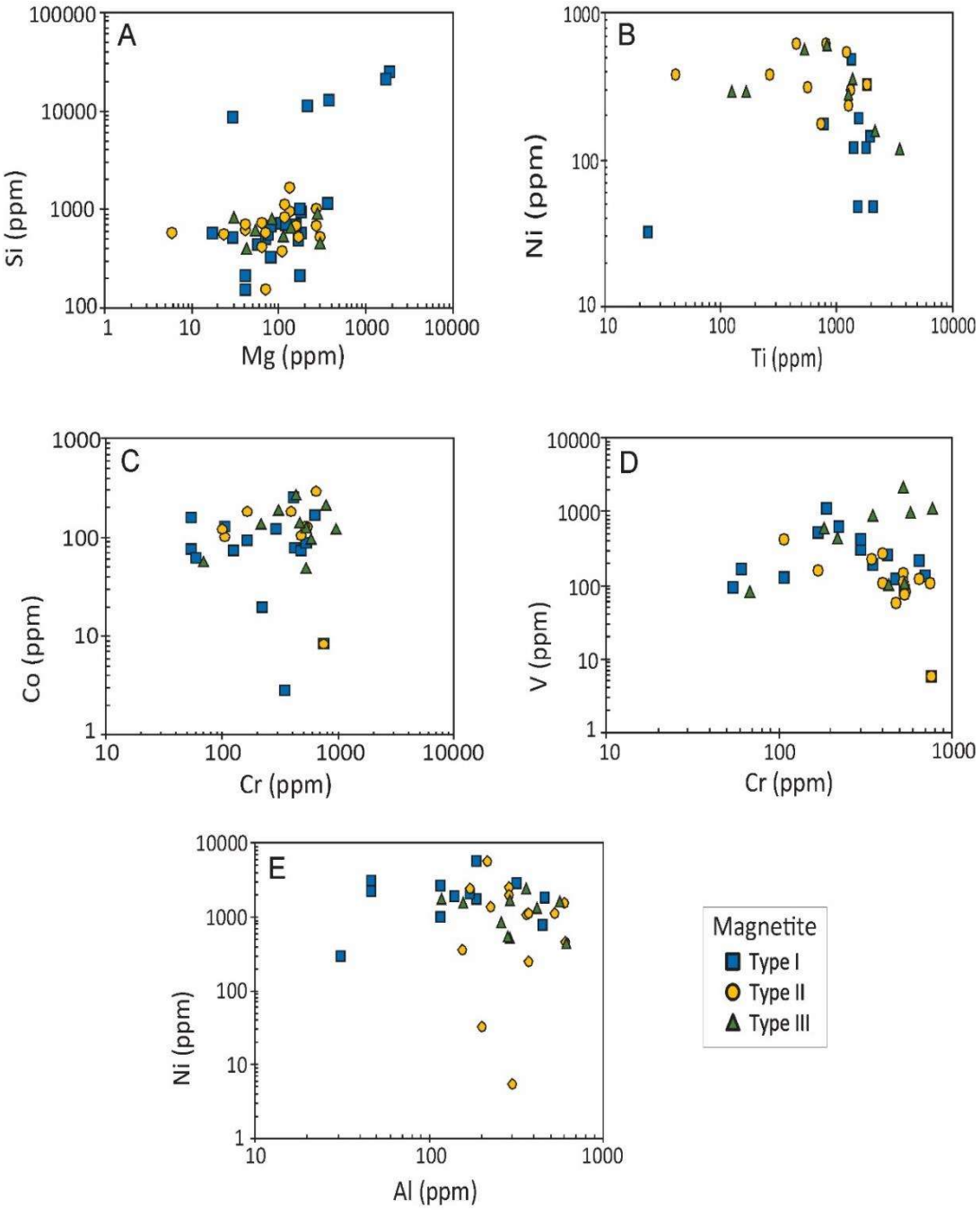

Fig. 8. Magnetite chemical data in ppm of the magnetite types (Mgt type I, II and type III) in binary plots. A. There is a similar Si and Mg concentration between the three magnetite types, some points of the Mgt type I present higher Si and Mg contents consistent with the association with Fe-rich silicates. B. Mgt type II present low Ni contents. C. Similar Co and Cr concentrations between the Mgt types. D. Mgt type III has, on average, the higher V concentrations. E. The Ni contents are generally below 600 ppm.

4.2 *Sulfur isotope data*

The $\delta^{34}S$ signature determined for the metamorphosed Salobo deposit were all from Cu-Fe-sulfides of the *chalcopyrite breccia* (Mgt type II), due to this samples shows an incipient hydrothermal alteration, thus allowing a better analysis of the primary sulfur composition. The pyrite, chalcopyrite and pyrrhotite cluster in a narrow range between 0.88 and 5.04 ‰ (Table 3; Fig. 9). The $\delta^{34}S$ results show variations related to two important textural-mineral chalcopyrite relationships; the first one (ccp 1) presents $\delta^{34}S$ ratios between 0.88 and 1.98‰ (mean $\delta^{34}S$= 1.56‰, σ= 0.12) and is linked to chalcopyrite (grains and inclusions) which in turn is associated with magnetite, pyrrhotite and pyrite (similar to Fig. 4C); and the second one (ccp 2) presents $\delta^{34}S$ ratios between 2.35 and 3.354‰ (mean $\delta^{34}S$= 2.73‰, σ= 0.11) and is related to a chalcopyrite matrix with subhedral pyrite grains (similar to Fig. 4E).

Clustering of the sulfur isotope data is evident for the ccp 1. There is no discernible difference between the pyrrhotite (mean $\delta^{34}S$= 1.57‰, σ= 0.1) and the chalcopyrite matrix (mean $\delta^{34}S$= 1.56‰, σ= 0.12). In contrast, the ccp 2 contains somewhat higher $\delta^{34}S$ ratios than those obtained from the ccp 1 ($\delta^{34}S_{V\text{-}CDT}$ values above 1.70‰), which also matches with the most positive sulfur isotope value 5.04‰ presented in pyrite grain that exhibit overgrown and chalcopyrite replacement (Similar to Fig. 4E). However, the ccp2 show lower $\delta^{34}S$ values than the precursor sulfide (i.e., pyrite; mean $\delta^{34}S$= 2.7 ‰, σ= 0.11). All isotopes values align with the mass-dependent fractionation line as no negative values or data related to the mass-independent fractionation was observed.

Table 3 - Sulfur isotopic values of Cu-Fe sulfides of the Salobo deposit.

Sample N°	Mineral	$\delta^{34}S_{V\text{-}CDT}$	± σ (‰)
SAL7C_1	Cpy	2,35	0,10
SAL7C_2		2,44	0,11
SAL7C_3		3,35	0,11
SAL7C_4		2,94	0,11
SAL7C_5		2,74	0,10
SAL7C_6		2,56	0,13
SAL7C_1	Py	2,17	0,11
SAL7C_2		2,12	0,11
SAL7C_3		5,04	0,11
SAL7C_4		3,36	0,11
SAL7C_5		1,83	0,11
SAL7C_6		1,70	0,11
SAL2A_1	Cpy	1,73	0,10
SAL2A_2		1,62	0,14
SAL2A_3		1,60	0,12
SAL2A_4		1,40	0,10
SAL2A_5		1,47	0,12
SAL2A_6		1,72	0,11
SAL2A_7		1,30	0,11
SAL2A_8		1,47	0,14
SAL2A_9		1,74	0,11
SAL2A_1	Po	1,88	0,09
SAL2A_2		1,95	0,09
SAL2A_3		1,98	0,10
SAL2A_4		1,90	0,09
SAL2A_5		1,64	0,09
SAL2A_6		1,55	0,09
SAL2A_7		1,56	0,10
SAL2A_8		1,45	0,09
SAL2A_9		0,95	0,11
SAL2A_10		1,62	0,10
SAL2A_11		1,31	0,09
SAL2A_12		1,42	0,10
SAL2A_13		1,83	0,09
SAL2A_14		0,88	0,12

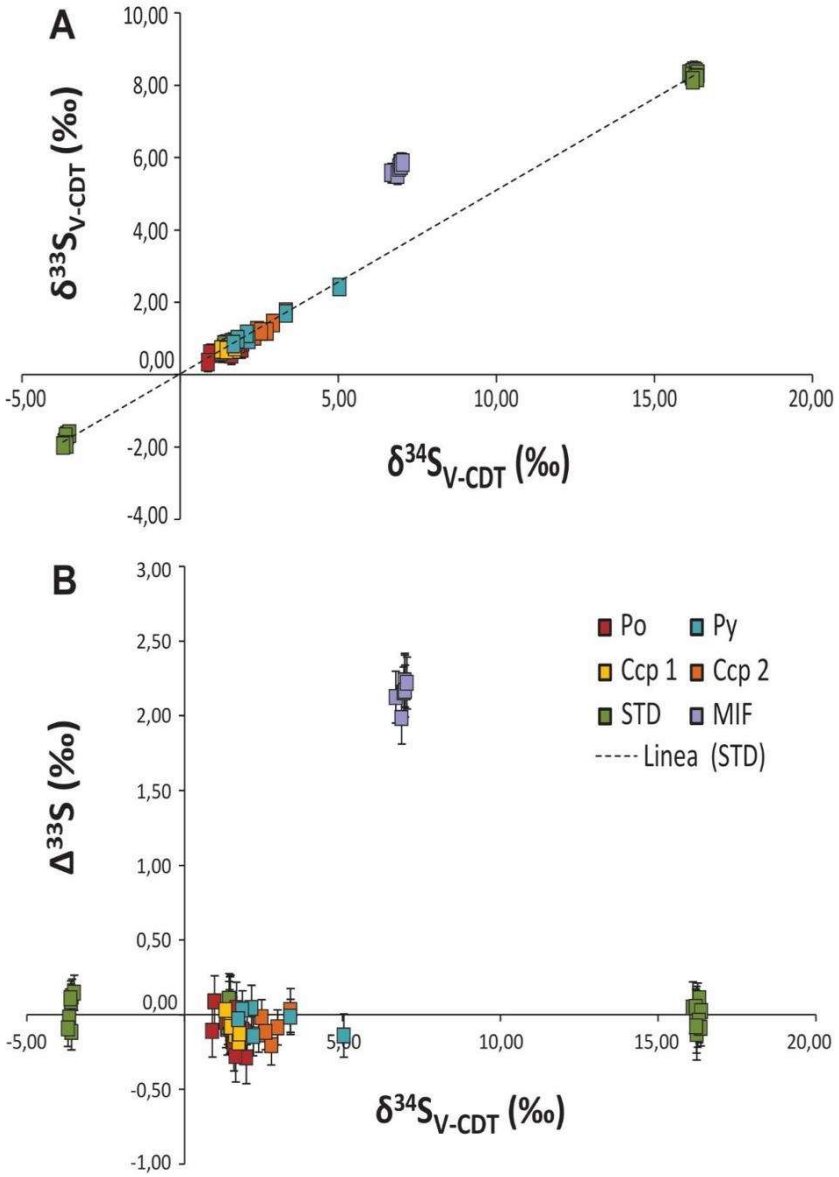

Fig. 9. Diagrams illustrating the distribution of pyrrhotine (po), pyrite (py) and the different chalcopyrite (ccp1 and ccp2) sulfur isotope data from the Salobo IOCG deposit. The data are grouped according to (A) values of $\delta^{33}S_{V\text{-}CDT}$ (‰) and (B) values of $\Delta^{33}S$ (‰). MIF: Sample laboratory standard pattern.

5 Discussion

5.1 *Discrimination diagrams for the magnetite origin at the Salobo deposit*

Recently, the geochemistry of magnetite from ore deposits systems including IOCG, IOA-Kiruna type, porphyry, and Fe-Ti-V, among others have been characterized in several composition discrimination diagrams using the magnetite as a fingerprint for mineral exploration (Dare et al., 2014; Dupuis and Beaudoin, 2011; Knipping et al., 2015; Nadoll et al., 2015, 2014; Wen et al., 2017). Even though the magnetite chemical measurements could be affected by the petrographic observations of textures, zonings and the presence/nature of mineral inclusions, besides, factors such as temperature, redox state and/or the partition coefficient (Broughm et al., 2017); these diagrams are a useful tool to discriminate and elucidate the iron-oxide origin among different ore deposit types and the different magnetite populations.

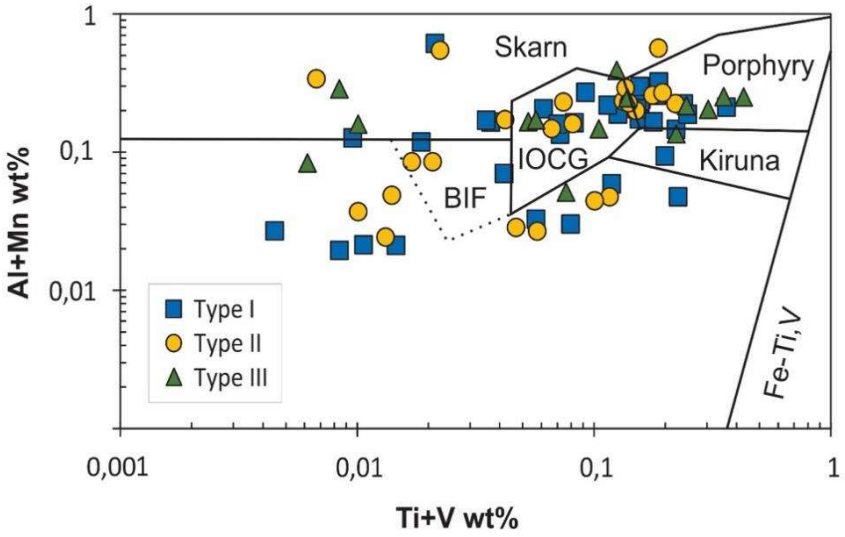

Fig. 10. Al+Mn vs. Ti+V discrimination diagram proposed by Dupuis and Beaudoin (2011) and modified by Nadoll et al. (2014), in which the chemical compositions of Mgt type I, II and type III are plotted.

We assess the chemical signature data (EPMA) from the crystallization stages at the Salobo deposit recorded in the three magnetite types (Mgt type I, II and type III) in one of the most used discriminant diagram proposed by Dupuis and Beaudoin, (2011) and later modified by Nadoll et al., (2014), in which Al, Mn, Ti and V abundances are used to distinguish magnetite from different mineral deposits (Fig. 10). The magnetite data do

not plot purely within the proposed IOCG discrimination box, conversely, significant points plotting within the porphyry field and some samples, of the three magnetite types, even extend into the BIF V field (Fig. 10). Texturally, the magnetite grains from Salobo are inclusion-rich, particularly the *magnetite-bearing breccia* – Mgt type II (Fig. 4C, D, 5), which is a feature that has been related to magmatic magnetite and produces elemental dispersion (Knipping et al., 2015). In contrast, the more variable dispersion of the Mgt type III could be the reflection of higher Ti and V concentration (125 – 3518 ppm Ti, 61 – 1098 ppm V; Fig. 6), which could be associated to the presence of ilmenite exsolutions in magnetite porphyroblasts related to garnet in the magnetite schist (Fig. 4G).

Hence, this diagram should be used with caution, it does not appear to be an ideal tool to understand the magnetite chemical relationships with the different kind of deposits. There is too much overlap between the deposits boxes to distinguish clearly a magnetite source, thus the difference of these Fe-oxide deposits needs to be more defined, having into account other important factors such as the element contribution from the host rocks, the different mineralized domains and styles of mineralization of the deposits (Dmitrijeva et al., 2019) and the magnetite textures and mineral-associations. However, since many of the magnetite points plots between the IOCG and porphyry zones, other authors suggest that the magnetite formation are similar to those observed in high-temperature hydrothermal systems, thus involve processes similar to those proposed for porphyry copper deposits (Knipping et al., 2015).

As the compositional range of magnetite from the Salobo IOCG deposit seem not to have a clear trend within the proposed fields of the previous diagram, we evaluate the magnetite V and Cr composition in a more recent identification plot proposed by Knipping et al., (2015). This plot is based on Cr vs. V concentrations to distinguish the Kiruna-type deposit from other high-temperature deposits (i.e., porphyry; IOCG and Fe-Ti, V; Fig. 11), since magnetite from IOCG has lower V concentrations related to Kiruna (IOA), and are enriched in Cr, as well as, porphyry and Fe-Ti, V deposits. Although most of the data, particularly of the Mgt type II magnetite does not plot in any proposed field, there is a closeness to the IOCG zone. While the Mgt type III shows a trend closer to the porphyry zone displaying again the slightly higher V concentrations of the magnetite grains with ilmenite exsolutions (Fig. 4G).

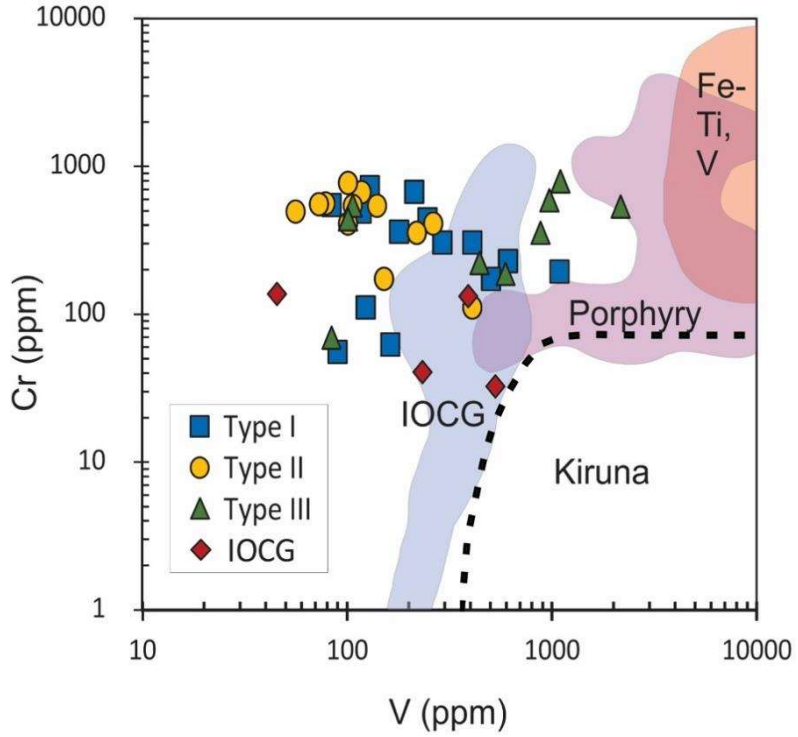

Fig. 11. The Cr vs. V concentration of the different magnetite types (Mgt type I, II and type III) from Salobo are plotted discriminating porphyry (pink), Fe-Ti, V (orange) and IOCG (blue) from Kiruna type, proposed by Knipping et al. (2015). The data source for IOCG from Dupuis and Beaudoin (2011), Dare et al. (2014) and Huang et al. (2019). See text for details.

Regarding with the IOA (Kiruna type) and IOCG relationship, the magnetite results for the Salobo deposit are following the descriptions of Knipping et al., (2015) and Rojas et al., (2018) for IOA deposits, namely, the Los Colorados and the EL Romeral, respectively. As shown by these authors the elevated V concentration and Cr-poor in IOA deposits are related to magnetite crystallization at high temperature, in contrast to magnetite from IOCG that are formed at moderately lower temperatures due to the hydrothermal influence. This difference can also be observed when comparing the results of this study with the IOA and IOCG compiled data from Huang et al., (2019) in Fig. 7, where besides to the Cr-V distinction is shown an enrichment in Mo, Cu, Y and Nb for IOCG deposits. Additionally, the higher Cr content IOCG in contrast with IOA could be the reflection of the high mobility of Cr^{+6} in high-temperature hydrothermal fluids (Knipping et al., 2015, and references therein) or augite fractionation in the magma source for a magmatic-hydrothermal fluid, which depletes the melt in Cr Rojas et al., (2018).

Conversely, the porphyry field denotes a greater V-enrichment referent to the IOCG zone. The elevated V concentration in magnetite from porphyry is consistent with magnetite crystallization at higher magmatic temperatures (Nadoll et al., 2015, 2014) than IOCG deposits. Despite the similar Cr content for both deposits, the Fe-bearing minerals allow distinguishing between this kind of deposits (Fe-sulfides for porphyry and Fe-oxides for IOCG, Richards and Mumin, 2013). In summary, this plot is more reliable for elucidating magnetite discrimination, when having into account the mineral assemblage especially for high-temperature Fe-deposits.

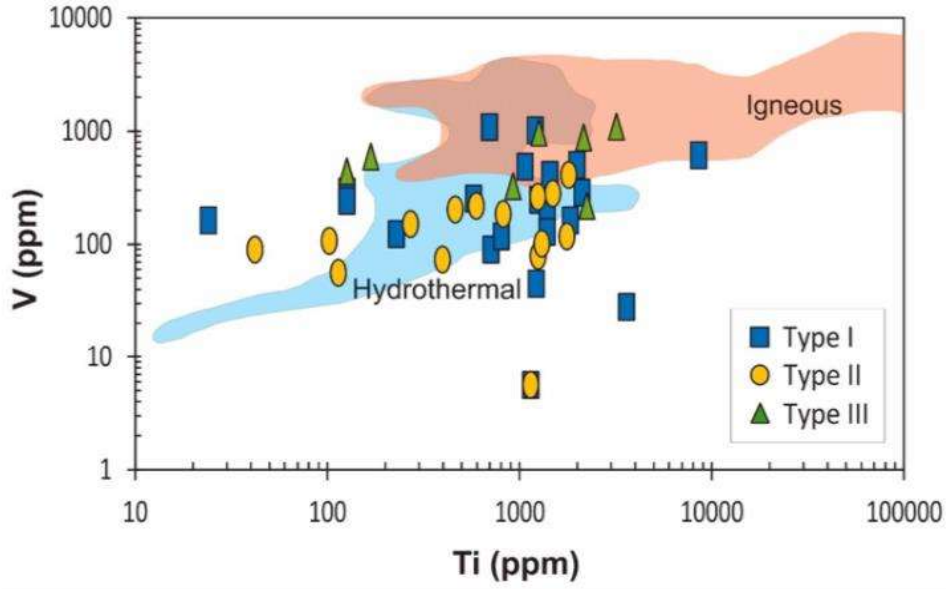

Fig. 12. The concentration of Ti vs. V diagram after Nadoll et al. (2014) with igneous and hydrothermal fields proposed by Knipping et al. (2015). Vanadium is relatively constant in Salobo magnetite type I and II, but high V-Ti concentrations are found in Mgt type III.

Furthermore, Nadoll et al., (2015) used V and Ti content to discriminate between igneous and magmatic-hydrothermal magnetite in porphyry systems (Fig. 12) owing to igneous magnetite is more enriched in these metals than hydrothermal ones. This diagram was used by Knipping et al., (2015) and Rojas et al., (2018), to support the magmatic-hydrothermal origin of magnetite-apatite deposits, drawing magmatic (igneous) and hydrothermal fields (Fig. 12). The concentrations of Mg between <100 – 232 ppm and Mn <100 – 1270 ppm of the Salobo magnetite are more consistent with igneous magnetite, as showing by Nadoll et al., (2015, 2014) the high Mg (>1 wt‰) and Mn contents (<100 – 50,400 ppm) are distinctive of hydrothermal magnetite, whereas the igneous magnetite present Mg concentration below of 3940 ppm and Mn between 102 –

12,500 ppm. Moreover, the Salobo magnetite (Mgt types I, II and III) contains Ti concentrations (23 to 3596 ppm; Fig. 6) overlapping the global average of igneous magnetite (<70 – 67100 ppm; Nadoll et al. 2014, 2015).

Nonetheless, the Salobo magnetite data are more related with the hydrothermal field (Fig. 11), the V concentrations (<100 – 1098 ppm) of the magnetite types are consistent with a high-temperature hydrothermal origin. Also, the slightly higher Fe and Co content (average of 91,58 wt% FeO and 391 ppm Co; table 2) denote a hydrothermal influence in the magnetite crystallization (Nadoll et al., 2015, 2014), and the Ti and V average (1242 and 308 ppm respectively, Fig. 7) are more sequent with the high-temperature hydrothermal magnetite values (<15 - 3380 ppm V and <15 – 3560 ppm Ti; Nadoll et al., 2015, 2014). Besides, Broughm et al., (2017) demonstrated that crystallization of magnetite from a melt may contain lower Ti concentration than is normal for igneous magnetite. Therefore, the ranges are more subsequent with a high-temperature magmatic-hydrothermal affinity for the Salobo magnetite rather than purely magmatic ones.

To determine the high-temperature magmatic-hydrothermal magnetite formation at Saloboa, we use the multielement variation diagram (Fig. 7) proposed by Dare et al., (2014), box and whiskers plots (Fig. 6) to help to highlight differences in the trace element composition and binary diagrams (Fig. 8) to reveal chemical compositional trends between the magnetite types. Referent to the deposits relationship, the distribution of Mn, Ti, Zn, Co, V, Ni, and Cr shows a correlation with the fields of porphyry and the high-temperature magmatic-hydrothermal (>500°C) deposits (Fig. 7), indicating that magnetite of the Salobo deposit grown from a high-temperature magmatic-hydrothermal fluid. Relating the magnetite results of this study to the data of Huang et al. (2019) for IOCG deposits, the chemistry of Salobo is significantly more enriched in W, Y, Zr, Hf, Ta, Ge and Sn, probably for the incorporation of micro zircon inclusions in Type II magnetite (Fig. 43D, 5) It should be noted that the Huang et al., (2019) samples are different from those used in this study. Nevertheless, the abundance of elements that typifying an IOCG geochemical signature, such as Si, Ti, Al, Mn, and V are in agreement with the IOCG field (Fig. 8), as well as the content of Ca, P, W, Mo, and Ni, which is also not consistent with a purely magmatic origin. Thus, the magnetite ore in Salobo likely formed from high-temperature fluids associated with an iron-rich magmatic-hydrothermal source, which is also highly enriched in lithophiles elements unlike others IOCG deposits (i.e., W, Y, Zr, Hf, Ta; Huang et al., 2019).

Regarding the diverse formation and alteration history of the magnetite types, Montreuil et al., (2016) showed that each hydrothermal alteration assemblage is associated with distinct element mobility patterns that record evolving physicochemical properties of the hydrothermal fluid. The mineral association of the Mgt type I with Fe-rich silicates (Fig. 4A, B) corresponds to the Ca-Fe alteration phase and the association of the Mgt type II with Cu-rich sulfides represents the Cu-(Fe) sulfide mineralization phase, both phases linked to the magmatic-hydrothermal mineralization stage. Nonetheless, the mineral assemblages of the Mgt type III that host the high-grade ore (Bornite, chalcocite, digenite; Vieira et al., 2019) present evidence from hydrothermal alteration and metamorphic-deformational events (Bernard Prado et al., 2019; Lindenmayer, 1990; Lindenmayer and Teixeira, 1999; Melo et al., 2019, 2017; Requia et al., 2003; Tassinari et al., 2003; Tavares et al., 2018; Vieira et al., 2019) like calcite-fluorite-hematite veins and deformed molybdenite (Fig. 4H, I), thus the Mgt type III is related to a low-grade metamorphism-deformation stage. Therefore, chemical variations in the magnetite signatures are expected as a response to the geological events and the mineral-textural relationships of each type.

In this context, the Cu values can be influenced by the association with chalcopyrite, which is reflected in the Mgt type II with a sulphide distribution of the Cu-mineralization (i.e., pyrite, chalcopyrite, bornite grains and inclusions). In the Mgt type II the copper values varying between 160 – 1638 ppm, besides, there is a slight enrichment in Zn and Zr concentration (ppm average 31282 Zn and 537 Zr). Thus, the enrichment in Cu and Zn content and particularly the higher Zr concentration in the Mgt type II (Fig. 6, 7), could be the result of the co-crystallization with Cu-Fe sulphides, as well as the abundant inclusions of uraninite and monazite (Fig. 4D, 5). This sulphide-magnetite assemblage in hydrothermal deposits indicates a sulphide magma saturation (Dare et al., 2014; Schlegel et al., 2017; Sun et al., 2015, 2013). As exemplified by Deditius et al., (2018), elements such as Ti, V, Si, Al, Ca, Mg, Na present within magnetite from hydrothermal ore deposits, tend to be either structurally incorporated into growth and sector zones or form mineral micro- to nano-sized particles, suggesting a supersaturation from a hydrothermal fluid, which in turn promotes exsolution of new phases from the mineral host. In this context, the inclusions of the Mgt type I and especially of the Mgt type II could have promoted during the metamorphic-deformational stage new mineral phases and thus the

subtle geochemical differences in the Mgt type III. Therefore, these subtle chemical variations cannot be a reliable parameter to defined different magnetite origins.

Conversely, the Mgt type III seems to retain the geochemical signature of the primary magmatic-hydrothermal mineralization (Mgt type I and II; Fig. 6, 7, 8). Despite the influence of the low-grade deformational metamorphism and the higher V and Ti contents (125 – 3518 ppm Ti, 61 – 1098 ppm V), the magnetite types (Mgt type I, II and III) shows the similar chemical distribution between them (Fig. 6, 7, 8). The Mgt type III present similar values with the others magnetite types in elements that characterize an IOCG deposit (i.e., Cr, Mg, Mn, Ti, Si and Al; Dare et al., 2014; Fig. 8). Moreover, Dmitrijeva et al., (2019) showed that the sulphide patterns of pyrite-chalcopyrite are relatively enriched in Ni-Co and depleted in bornite-chalcocite patterns; whereby would be expected an outstanding difference between Ni-Co concentrations of the Mgt type II and type III, according to the mineral assemblage; chalcopyrite matrix with pyrite and pyrrhotite for the Mgt type II and bornite-chalcocite veins for the Mgt type III. Nevertheless, both magnetite types present similar Ni-Co concentrations (Fig. 7).

The chemical similarity between the magnetite types suggests that the Mgt type I, II, and III shares the same magmatic-hydrothermal composition, ergo, that the Mgt type III could be the result of magnetite recrystallization of the Mgt type I and II probably induced by the metamorphic and magmatic-hydrothermal events, following the deformation/metamorphism and magmatism recorded in the Salobo deposit at ~2.5 Ga (Machado et al., 1991; Melo et al., 2017; Pinheiro and Holdsworth, 2000; Requia et al., 2003; Tassinari et al., 2003). Hence, recrystallization evidence is expected to see in the Mgt type III, in fact, the granoblastic this magnetite type exhibit 120° triple junctions, feature attributed to this process (Huang and Beaudoin, 2019 and references therein; Urai et al., 1986). However, the Mgt type III lacks another important feature such as the undulant extinction, which could be a result of later Paleoproterozoic remobilization events associated with magmatism (Lindenmayer and Teixeira, 1999; Machado et al., 1991; Melo et al., 2017; Pollard et al., 2018; Requia et al., 2003; Tassinari et al., 2003), which are represented in the Mgt type III by discordant veins of bornite, digenite, chalcocite, covellite, fluorite, calcite and hematite (Fig. 4H, I). These veins are also associated with graphite. The bornite exhibits exsolutions textures of lower-temperature phases (i.e., chalcocite and digenite; Fig. 4I, 14C) from a bornite solid solution. It should be noted that no magnetite is attributed to this late overprinting and the predominant Fe-

oxide is hematite, that can be either a magnetite weathering product or from late-stage hydrothermal alteration.

In summary, seemingly the magnetite chemistry at Salobo is not influenced by the low-grade metamorphism and/or meta-somatic alteration as suggested by the similarities in the chemistry signature between the magnetite types, which also indicates that the metamorphic event resulted in recrystallization of the previous mineralogical phases, instead of a new generation of mineral assemblies from another source. This is following Vieira et al., (2019), as shown by these authors the ore event sequence for the Salobo deposit includes three-stages, namely, an early IOCG type magmatic-hydrothermal ore formation (2.74 – 2.73 Ga), which is overprinted by a metamorphic deformational stage (2,55 Ga) and a late thermal remobilization stage (Paleoproterozoic). In this context, the Salobo would represent a case of metamorphosed Neoarchean IOCG-type deposit, ergo, the magnetite type III assembly characterized by *foliated magnetite* (Fig. 4G, 14B) with biotite and almandine is interpreted as products of metamorphosed Ca-Fe alteration recorded in magnetite types I and II (*massive magnetite* and *magnetite-bearing breccia*, respectively).

5.2 *Sulfur isotopic evidence*

The reduced and/or oxidized sulfur species in the mineralizing fluid, as well as the sulfur isotope composition of its source, are reflected by the $\delta^{34}S$ values of sulfide minerals (Rye, 1993; Schlegel et al., 2017). The isotopic grouping of the $\delta^{34}S$ data, namely, ccp 1 (mean $\delta^{34}S$= 1.56‰, σ= 0.12) and ccp2 (mean $\delta^{34}S$= 2.73‰, σ= 0.11) above mentioned (Fig. 9), shows a small isotopic gradient at the site of the Cu-Fe sulfides deposition, suggesting that the $\delta^{34}S$ values of chalcopyrite (ccp-py assemblage) are partly inherited from the associated pyrite (Schlegel et al. 2017, and references therein). In other words, part of the chalcopyrite formation could have been driven by reaction of pyrite with an oxidized Cu-rich fluid resulting in a replacement of pyrite by chalcopyrite (Fig. 4E) during the same Cu-Au mineralization event. Moreover, the $\delta^{34}S$ values of the precursor pyrite could be affected by the pyrite replacement resulting in a more positive sulfur isotope value 5.04‰ (similar to Fig. 4E; Schlegel et al. 2017).

Likewise, the $\delta^{34}S$ pyrite values reflect equilibrium precipitation with the chalcopyrite, typically at high-temperature conditions, whereas the anhedral and massive chalcopyrite matrix (similar to Fig. 4C, F) may represent non-replaced pyrite showing similar but lower $\delta^{34}S$ values (Fig. 9). Thus, isotopic disequilibrium is assumed between Cu-sulfide pairs and the replaced pyrite, while isotopic equilibrium is showed by the texturally coexisting magnetite-chalcopyrite. These isotopic features suggest that the same high-temperature magmatic-derived fluid at magmatic-hydrothermal stage (or the Cu-mineralizing stage, the *magnetite-bearing breccia* – Mgt type II) formed at least two generations of Cu-sulfides with very similar $\delta^{34}S_{V\text{-}CDT}$ values, namely, textural chalcopyrite replacing pyrite and associated chalcopyrite that do not replace early pyrite.

Moreover, the Cu-Fe sulphides show $\Delta^{33}S$ values close to zero and plot within their errors on the terrestrial sulfur fractionation line (Fig. 9B), that is no MIF results, indicating an endogenic source for the mineralizing fluid without atmospheric conditions (exogenic sulfur cycle) influence (Halevy et al., 2010; Johnston, 2011; Rye, 1993), according to Bühn et al., (2012) who demonstrated the necessity that in Archean sulfide deposits the sulfur has to derive from the exogenic sulfur cycle to record a mass-independent fractionation (MIF) effect.

Furthermore, the no negative or broad range in $\delta^{34}S$ results suggests that the fluid could not have interacted with evaporites or calcareous host rocks (Rye 1993; Schlegel et al. 2017, and references therein), thus a single sulfur source. As exemplified by Schlegel et al. (2017), a narrow range in the $\delta^{34}S_{V\text{-}CDT}$ values can be produced by SO_2 disproportionation from a magmatic-hydrothermal fluid dominated by moderately reduced sulfur, another perspective of the conventional model in which diverse sulfur sources are a requirement for IOCG style mineralization. In summary, the narrower range of the $\delta^{34}S$ results (0.88 to 5.04‰; Fig. 9) points to a mainly magmatic sulfur source without/or minimal external fluids contributions.

5.3 *Formation conditions for Cu-(Fe) sulfide phase*

To elucidate the mineralization processes that generated the ore in the Salobo deposit, it is essential to know the geochemical behaviour of Sulfur, due to its importance as

geosolvent that controls the behaviours of copper and other chalcophile elements (Sun et al., 2015, 2004, 2013). Typically, sulfate is more soluble than sulphide in magnetite-saturated magmas with normal to high fO_2 (Rye, 1993; Sun et al., 2015). Redox conditions and closed system decompressional magma degassing controls the SO_2/H_2S ratios in the magmatic volatile phase (Schlegel et al., 2017; Vigneresse et al., 2019), which in turn is related to the oxidation state and the fO_2 (Schlegel et al., 2017; Sun et al., 2015, 2004, 2013) upon which the sulfate reduction in the oxidized magma source depends (Sun et al., 2013). For the Cu-mineralization is very important the sulfate reduction phase because it scavenges copper and other chalcophile elements out of the magma into ore-forming fluids and subsequently transports the metals for forming deposits (Sun et al., 2004, 2013).

It has been proposed that the sulfate reduction in oxidized magmas starts with ferrous iron oxidation during magnetite crystallization (i.e., *magnetite crisis*; Jenner et al. 2010; Fig. 13), accompanied by high oxygen fugacity and decreasing pH (Sun et al., 2015, 2013). As shown by Sun et al., (2015) ferrous iron is the principal reducing agent in highly oxidized magmas, because CO_2 or H_2O and SO are already oxidized in the early magma evolution. Moreover, as illustrated by Jenner et al., (2010), the appearance of magnetite in the melt at ~60 wt‰ SiO_2 and Mg ~$40_{(tot\ rock)}$, decreases the de $FeO_{(tot)}$, switching the dissolved S from SO_4^{2-} to S^{2-}, thus generating the magmatic sulfur disproportionation.

In this context, oxidation promotes the sulfur disproportionation (Fig. 13) in the magma source increasing initial chalcophile element concentrations (Sun et al., 2013). Oxidation is better described as oxidation of ferrous Fe (Eq. 1) and FeO-bearing minerals (Eq. 2) by sulfate or another oxidant (Schlegel et al., 2017; Sun et al., 2015, 2004):

$$SO_4^{2-} + 8Fe^{2+} + 8H_2O = 4Fe_2O_3 + S^{2-} + 16H^+ \qquad (1)$$

$$SO_2 + 6FeO + H_2O = H_2S + 3\,Fe_2O_3 \qquad (2)$$

Indeed, this sulfate reduction reaction provides S^{2-} and promotes the formation of pyrite (Eq. 3) and chalcopyrite (Eq. 4) (Sun et al. 2015, and references therein):

$$Fe^{2+} + 2H_2S = FeS_2 + 2H^+ + H_2 \qquad (3)$$

$$2Cu^{+} + 2Fe^{2+} + 4H_2S = 2CuFeS_2 + 6H^{+} + H_2 \qquad (4)$$

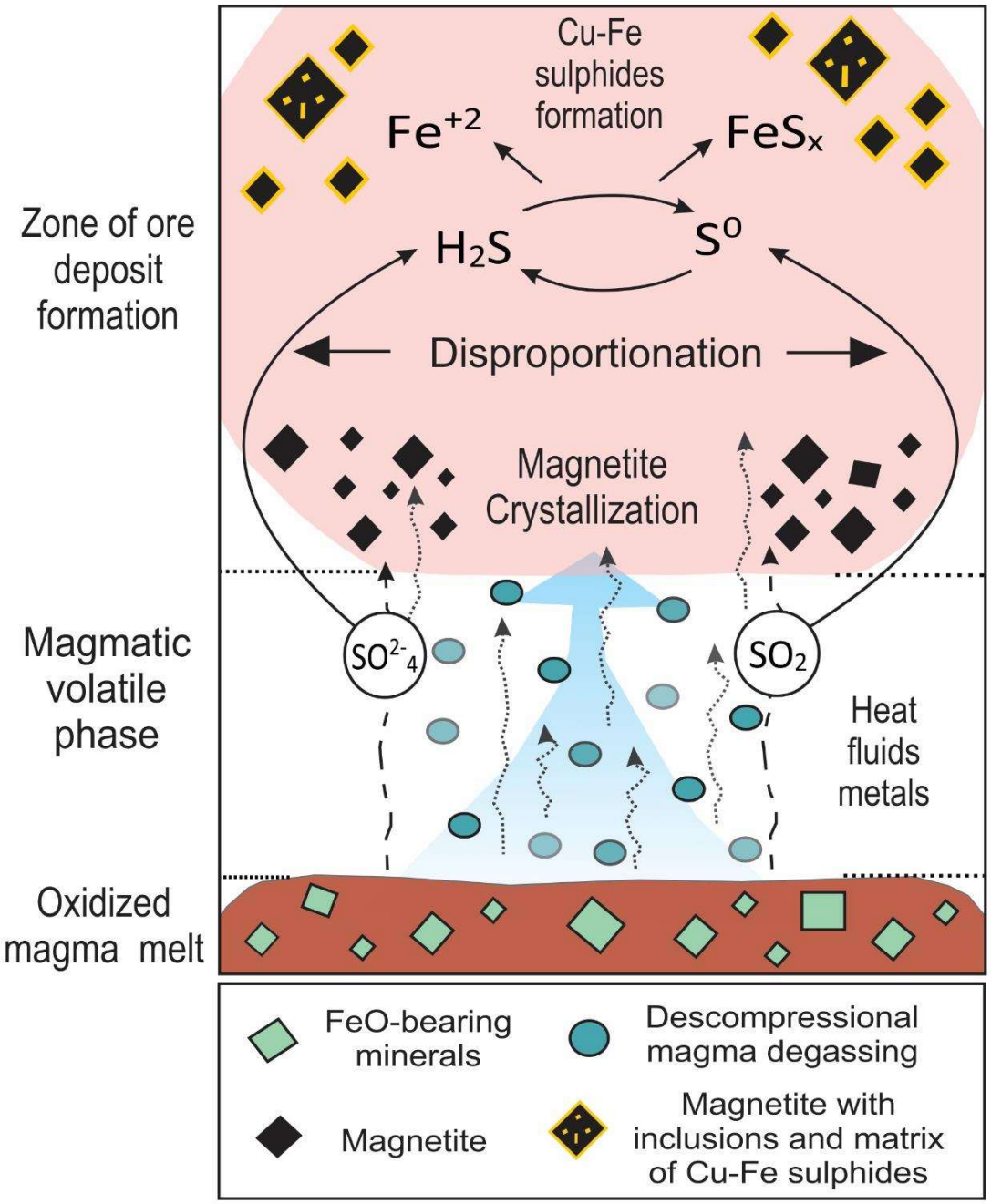

Fig. 13. Schematic diagram illustrating the role of the magnetite crystallization in the sulfur disproportionation process.

Thereby, it is common that magnetite formed during this process coexists with sulphides (Fig. 4C, 5, 13, 14; Sun et al. 2013) as well as, includes chalcopyrite and bornite inclusions, which in turns is usually concomitant with the apatite appearance (Fig. 4D, 5; Gelcich et al. 2005; Jenner et al. 2010). However, according to the chalcopyrite-pyrite

textures (Fig. 4E), part of the chalcopyrite formation could have been driven by a reaction of pyrite with an oxidized Cu-rich fluid resulting in pyrite replacement, according to the Eq. 5 (Schlegel et al., 2017):

$$2FeS_2 + Cu^{2+} + 8H_2O = CuFeS_2 + Fe^{2+} + 2SO_4^{2-} + 4H^+ + 6H_2 \quad (5)$$

In summary, the oxidized nature of the magma is of crucial importance to crystallizes magnetite onto the liquidus in the early magma evolution, which induces the sulfate reduction to sulphides and thus generating the Cu-mineralization (Fig. 13), besides replacement of pre-ore sulphides can contribute to the Cu-enrichment. In other words, the same magmatic S-bearing fluid evolving along oxidized and reduce chemical paths could be the key process to produce the Cu-IOCG style mineralization at Salobo, without shallow or surficial sulfur contribution (e.g., meta-sedimentary and evaporite rocks) as a must-have rule as in previous genetic models proposed for IOCG systems in Carajás and others deposits that promotes multiple and diverse sulfur sources (Barton, 2014).

5.4 *A magmatic-hydrothermal model for the Salobo deposit*

The petrographic evidence (Fig. 4) supports a three-magnetite textural-growing phase linked to the magmatic evolution related to the Salobo deposit in the Carajás Mineral Province (Fig. 14). During Neoarchean volcanism (before to ~2.5 Ga) a high-temperature magmatic-hydrothermal oxidized magnetite-forming fluid shaped the first pre-ore stage, the *massive magnetite* – Mgt type I (Ca-Fe alteration, Fig. 14A).

According to the presence of high-temperature minerals associated with magnetite (i.e., fayalite and ferrosilite; Fig. 4A, B), the $\delta^{34}S$ values observed (Fig. 9) and the magnetite chemical signature (Fig. 6, 7, 8); the crystallization of magnetite during the magma differentiation caused ferrous Fe oxidation. Thereby, the magnetite precipitation triggered the magmatic sulfur disproportionation and thus the sulfate reduction, promoting the formation of Cu-Fe sulphides (i.e., chalcopyrite and pyrite; Fig. 13) in the later or at least outlasting *magnetite-bearing breccia* – Mgt type II (Cu-mineralizing stage; Fig. 14A). Indeed, the type II magnetite is associated with Cu-Fe sulphides (Fig. 4, 5), but also one fraction of the chalcopyrite precipitation occurred by a reaction of Cu-bearing fluid with a reductant containing Fe^{2+} (i.e., pyrite replacement) according to the

narrower sulfur signature (Fig. 9) and ore textures (Fig. 4) similar as occurs in high-temperature and low-pressures oxidized-hydrothermal systems (Rye, 1993; Schlegel et al., 2017; Sun et al., 2015).

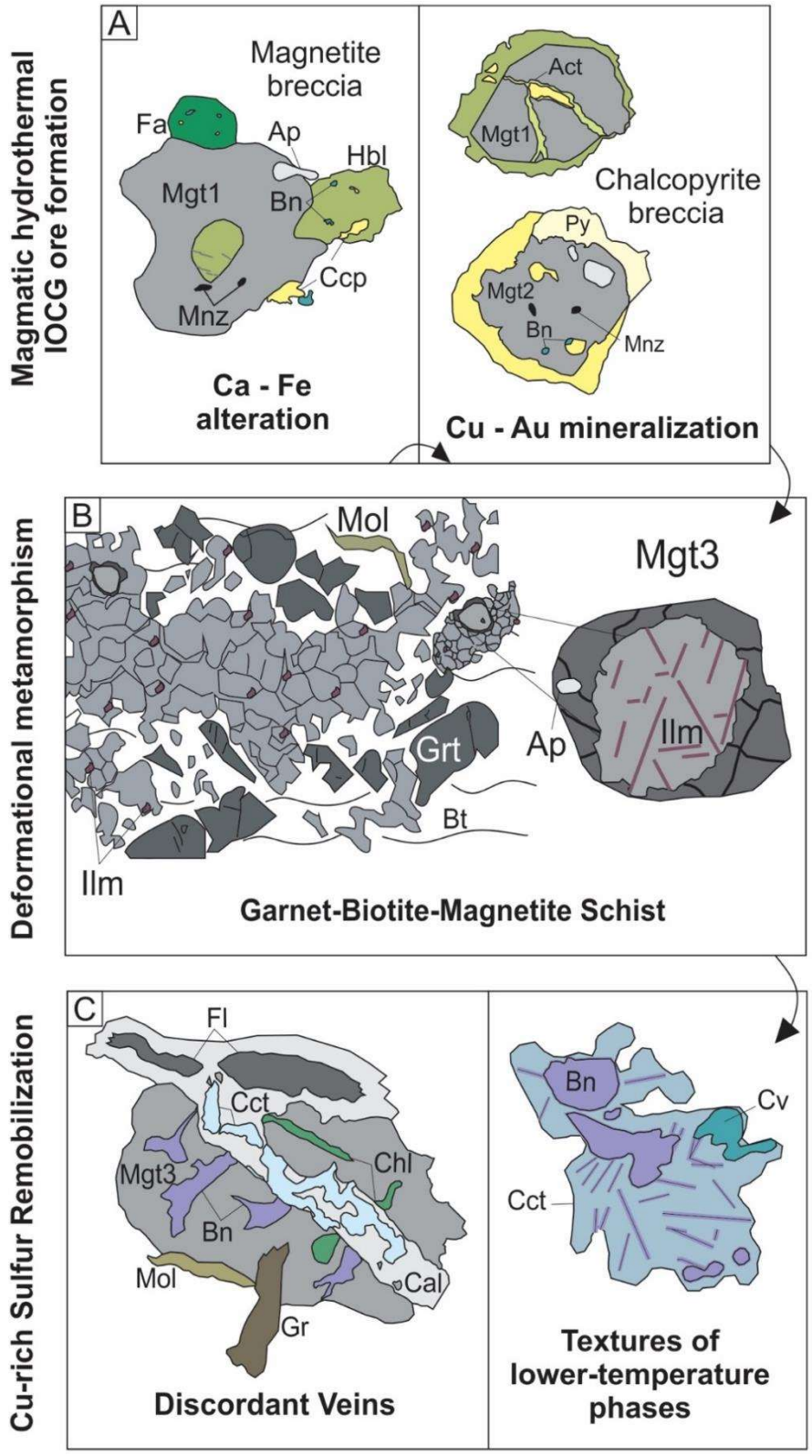

Fig. 14. Schematic diagram illustrating the three-sulfide magnetite textural-growing stages, and its relationship with the mineralization processes, which are (A) magmatic-hydrothermal IOCG ore formation (*massive magnetite* – Mgt type I*, magnetite-bearing breccia* – Mgt type II*)*; (B) Deformational metamorphism (*magnetite schist* – Mgt type III) and (C) Cu-rich sulfur remobilization. Mineral abbreviations: Act: Actinolite. Ap: Apatite. Bn: Bornite. Cal: Calcite. Cct: Chalcocite. Ccp: Chalcopyrite. Chl: Chlorite. Cv: Covellite. Fa: Fayalite. Fl: Fluorite. Grt: Garnet. Gr: Graphite. Hbl: Hornblende. Ilm: Ilmenite. Mgt: Magnetite. Mnz: Monazite. Mol: Molybdenite. Py: Pyrite.

We suggest that the mineralizing fluid did not interact with the oxidized surface or subsurface environment and none or minimal external fluid influence was presented, in agreement with no mass-independent fractionation and narrower $\delta^{34}S$ results (Fig. 9; Rye, 1993). Therefore, the two generations of Cu-rich sulfides resulted in chalcopyrite-rich breccias at the Cu-mineralizing stage, indicating that the highly oxidized fluid containing dominantly magmatic solute components including copper, may however, have been enough to contribute to the bulk Cu grade in Salobo.

Then during the later medium-low metamorphic events at ca. ~2.55 Ga associated with the tectonic reactivation of Carajás Cinzento Shear Zone (Tassinari et al., 2003), the previous Fe-Cu-rich stages undergone magnetite remobilization and recrystallization resulting in the granoblastic *magnetite schist* – Mgt type III assemblage (Fig. 4G, 14B), thus inheriting the trace element signatures. Finally, we suggest that the Paleoproterozoic alkaline to sub–alkaline A-type magmatism (Lindenmayer and Teixeira, 1999; Machado et al., 1991; Pollard et al., 2018), produced ore-sulfur remobilization of the Cu-rich sulphides (Fig. 14C), which is expressed in discordant veins of bornite, digenite, chalcocite, covellite, fluorite and calcite in the magnetite-rich schists (Fig. 4H, I). This remobilization did not produce a new overprinting of magnetite, conversely, it is characterized by a sulfur concentration (Vieira et al., 2019).

6 Conclusions

Magnetite from the Salobo IOCG deposit crystallizes in three different textures regarding the mineralizing stages. The primary mineralization was formed from the magmatic fluid

under non-oxidizing atmospheric or crustal conditions generating the *massive magnetite* – Mgt type I (Ca-Fe alteration) and the *magnetite-bearing breccia* – Mgt type II (Cu-Au mineralization), both related to the magmatic-hydrothermal stage in the Neoarchean (before to ~2.5 Ga).

The magnetite trace element signature and the total spectrum of sulfur isotope compositions of sulfides in the magmatic-hydrothermal stage can be explained by the first crystallization of magnetite, whose saturation-fractionation triggered the sulfate reduction allowing the Cu-Fe sulphides precipitation. Moreover, some pyrite-replacement reflects that part of the chalcopyrite crystallization could have been driven by a Cu-rich oxidized magma fluid reacting with a reductant Fe of early pyrite, contributing to the Cu-grade ore in Salobo. Subsequent metamorphism related to the emplacement of the Old Salobo Granite, due to the Cinzento Shear Zone reactivation in ca. ~2.5 Ga generated the recrystallized granoblastic *magnetite schist* – Mgt type III, which underwent late remobilization and sulfur re-concentration at the Paleoproterozoic resulting discordant veins of bornite, chalcocite and digenite and exsolutions textures of chalcocite-covellite in bornite.

Thus, although the main Cu mineralization characterized by Cu-sulfides assemblages (i.e., bornite, chalcocite and digenite) and magnetite, is related to the late metamorphism and remobilization event hosted in the magnetite schist, the primary Cu mineralization at Salobo was developed during the magmatic-hydrothermal stage in a Cu-rich sulfide chalcopyrite-breccia, who underwent metamorphism resulting in the "unusual" ore mineralogy dominated by an association of magnetite-bornite-chalcocite characteristic of Salobo.

The data contributes to the understanding of the processes that led to the formation of the ore. The distribution of magnetite chemistry in discriminant diagrams does not allow a clear distinction in the deposit origin, however, they show that the different magnetite types have a similar geochemical signature despite the different geological-metallogenic events to which they are associated. Therefore, the Mgt type III resulted from recrystallization of the previous magnetite types I and II. Based on the results of sulfur isotopes and the textural relationships of the analysed sulphides, the origin of the Cu-bulk t is related to a high-temperature magmatic-hydrothermal sulfur source that evolved along oxidizing and reducing pathways during the mineralization stages

without/or minimal sulfur contributions. Our results suggest an ore formation model of IOCG type that involves processes similar to those that occur in high-temperature magmatic-hydrothermal systems such as porphyry, called "*magnetite crisis*", contributing to the understanding of the mineralization genesis in IOCG type deposits.

Acknowledgements

Dr Martin Whitehouse and Dr Heejin Jong are especially appreciated for analytical support. We also would like to thank the VALE for providing access to the company's data and for supporting field activities, as well as to the Instituto de Geociências of the University of Brasília for the analytical facilities. Maria Emilia Schutesky and Claudinei Gouveia acknowledge the CNPq for continuous funding through research grants. This study is part of the first author's (Yuri Tatiana Campo Rodríguez) M.Sc. dissertation developed at the University of Brasília, which was financed in part by the Coordenação de Aperfeiçoamento de Pessoal de Nível Superior - Brasil (CAPES) - Finance Code 001 and by the Swedish Research Link Programme.

References

Acosta-Góngora, P., Gleeson, S.A., Samson, I.M., Corriveau, L., Ootes, L., Jackson, S.E., Taylor, B.E., Girard, I., 2018. Origin of sulfur and crustal recycling of copper in polymetallic (Cu-Au-Co-Bi-U ± Ag) iron-oxide-dominated systems of the Great Bear Magmatic Zone, NWT, Canada. Miner. Depos. 53, 353–376. https://doi.org/10.1007/s00126-017-0736-6

Avelar, V.G., Lafon, J.M., Correia Jr., F.C., Macambira, E.M.B., 1999. O magmatismo arqueano da região de Tucumã - Província Mineral De Carajás: Novos resultados geocronológicos. Rev. Bras. Geociências 29, 453–460.

Barton, M.D., 2014. Iron Oxide(-Cu-Au-REE-P-Ag-U-Co) Systems, 2nd ed, Treatise on Geochemistry: Second Edition. Elsevier Ltd. https://doi.org/10.1016/B978-0-08-

095975-7.01123-2

Biagioni, C., Pasero, M., 2014. The systematics of the spinel-type minerals: An overview. Am. Mineral. 99, 1254–1264. https://doi.org/10.2138/am.2014.4816

Broughm, S.G., Hanchar, J.M., Tornos, F., Westhues, A., Attersley, S., 2017. Mineral chemistry of magnetite from magnetite-apatite mineralization and their host rocks: examples from Kiruna, Sweden, and El Laco, Chile. Miner. Depos. 52, 1223–1244. https://doi.org/10.1007/s00126-017-0718-8

Bühn, B., Santos, R. V., Dardenne, M.A., de Oliveira, C.G., 2012. Mass-dependent and mass-independent sulfur isotope fractionation (δ34S and δ33S) from Brazilian Archean and Proterozoic sulfide deposits by laser ablation multi-collector ICP-MS. Chem. Geol. 312–313, 163–176. https://doi.org/10.1016/j.chemgeo.2012.04.003

Chen, H., 2013. External sulphur in IOCG mineralization: Implications on definition and classification of the IOCG clan. Ore Geol. Rev. 51, 74–78. https://doi.org/10.1016/j.oregeorev.2012.12.002

Dare, S.A.S., Barnes, S.J., Beaudoin, G., Méric, J., Boutroy, E., Potvin-Doucet, C., 2014. Trace elements in magnetite as petrogenetic indicators. Miner. Depos. 49, 785–796. https://doi.org/10.1007/s00126-014-0529-0

Deditius, A.P., Reich, M., Simon, A.C., Suvorova, A., Knipping, J., Roberts, M.P., Rubanov, S., Dodd, A., Saunders, M., 2018. Nanogeochemistry of hydrothermal magnetite. Contrib. to Mineral. Petrol. 173, 1–20. https://doi.org/10.1007/s00410-018-1474-1

Delinardo da Silva, M.A., 2014. Metatexitos e Diatexitos do Complexo Xingu na região de Canaã dos Carajás: Implicações para a evolução mesoarqueana do domínio Carajás. Universidade Estadual de Campinas, Brazil.

Dmitrijeva, M., Ehrig, K.J., Ciobanu, C.L., Cook, N.J., Verdugo-Ihl, M.R., Metcalfe, A. V., 2019. Defining IOCG signatures through compositional data analysis: A case study of lithogeochemical zoning from the Olympic Dam deposit, South Australia. Ore Geol. Rev. 105, 86–101. https://doi.org/10.1016/j.oregeorev.2018.12.013

DOCEGEO, 1988. Revisão litoestratigráfica da Província Mineral de Carajás - Litoestratigrafia e principais depósitos minerais. Congr. Bras. Geol. 35th, 11–54.

Droop, G.T.R., 1987. A general equation for estimating Fe 3+ concentrations in ferromagnesian silicates and oxides from microprobe analyses, using stoichiometric criteria. Mineral. Mag. 51, 431–435. https://doi.org/10.1180/minmag.1987.051.361.10

Dupuis, C., Beaudoin, G., 2011. Discriminant diagrams for iron oxide trace element fingerprinting of mineral deposit types. Miner. Depos. 46, 319–335. https://doi.org/10.1007/s00126-011-0334-y

Feio, G.R.L., Dall'Agnol, R., Dantas, E.L., Macambira, M.J.B., Santos, J.O.S., Althoff, F.J., Soares, J.E.B., 2013. Archean granitoid magmatism in the Canaã dos Carajás area: Implications for crustal evolution of the Carajás province, Amazonian craton, Brazil. Precambrian Res. 227, 157–185. https://doi.org/10.1016/j.precamres.2012.04.007

Gelcich, S., Davis, D.W., Spooner, E.T.C., 2005. Testing the apatite-magnetite geochronometer: U-Pb and 40Ar/ 39Ar geochronology of plutonic rocks, massive magnetite-apatite tabular bodies, and IOCG mineralization in Northern Chile. Geochim. Cosmochim. Acta 69, 3367–3384. https://doi.org/10.1016/j.gca.2004.12.020

Gleeson, S.A., Smith, M.P., 2009. The sources and evolution of mineralising fluids in iron oxide-copper-gold systems, Norrbotten, Sweden: Constraints from Br/Cl ratios and stable Cl isotopes of fluid inclusion leachates. Geochim. Cosmochim. Acta 73, 5658–5672. https://doi.org/10.1016/j.gca.2009.06.005

Groves, D.I., Bierlein, F.P., Meinert, L.D., Hitzman, M.W., 2010. Iron Oxide Copper-Gold (IOCG) Deposits through Earth History: Implications for Origin, Lithospheric Setting, and Distinction from Other Epigenetic Iron Oxide Deposits. Econ. Geol. 105, 641–654. https://doi.org/10.2113/gsecongeo.105.3.641

Halevy, I., Johnston, D.T., Schrag, D.P., 2010. Explaining the Structure of the Archean Mass-Independent Sulfur Isotope Record, Science. https://doi.org/10.1192/bjp.177.1.47

Hitzman, M.W., Oreskes, N., Einaudi, M.T., 1992. Geological characteristics and tectonic setting of proterozoic iron oxide (CuUAuREE) deposits. Precambrian Res. 58, 241–287. https://doi.org/10.1016/0301-9268(92)90121-4

Huang, X., Boutroy, É., Makvandi, S., Beaudoin, G., Corriveau, L., Toni, A.F. De, 2019. Trace element composition of iron oxides from IOCG and IOA deposits : relationship to hydrothermal alteration and deposit subtypes. Miner. Depos. 54, 525–552.

Huang, X.W., Beaudoin, G., 2019. Textures and chemical compositions of magnetite from iron oxide copper-gold (IOCG) and kiruna-type iron oxide-apatite (IOA) deposits and their implications for ore genesis and magnetite classification schemes. Econ. Geol. 114, 953–979. https://doi.org/10.5382/econgeo.4651

Huhn Bacelar, S.R., 1996. São os depósitos cupríferos de Carajás do tipo Cu-Au-U-(ETR)?, in: Sociedade Brasileira de Geologia, N.N. (Ed.), Boletim de Resumos Expandidos e Guia de Excursões. Belém - Pará, pp. 140–143.

Jenner, F.E., O'Neill, H.S.C., Arculus, R.J., Mavrogenes, J.A., 2010. The magnetite crisis in the evolution of arc-related magmas and the initial concentration of Au, Ag and Cu. J. Petrol. 51, 2445–2464. https://doi.org/10.1093/petrology/egq063

Johnston, D.T., 2011. Multiple sulfur isotopes and the evolution of Earth's surface sulfur cycle. Earth-Science Rev. 106, 161–183. https://doi.org/10.1016/j.earscirev.2011.02.003

Knipping, J.L., Bilenker, L.D., Simon, A.C., Reich, M., Barra, F., Deditius, A.P., Wälle, M., Heinrich, C.A., Holtz, F., Munizaga, R., 2015. Trace elements in magnetite from massive iron oxide-apatite deposits indicate a combined formation by igneous and magmatic-hydrothermal processes. Geochim. Cosmochim. Acta 171, 15–38. https://doi.org/10.1016/j.gca.2015.08.010

Lindenmayer, Z.G., 1990. Salobo sequence, Carajás, Brasil: Geology, geochemistry and metamorphism. Western University.

Lindenmayer, Z.G., Teixeira, J.B.G., 1999. Ore genesis at the Solobo copper deposit, Serra dos Carajás. Base Met. Depos. Brazil 33–43.

Machado, N., Lindenmayer, Z., Krogh, T.E., Lindenmayer, D., 1991. U-Pb geochronology of Archean magmatism and basement reactivation in the Carajás area, Amazon shield, Brazil. Precambrian Res. 49, 329–354. https://doi.org/10.1016/0301-9268(91)90040-H

Melo, G.H.C. de, Monteiro, L.V.S., Xavier, R.P., Moreto, C.P.N., Santiago, E., 2019. Tracing fluid sources for the salobo and Igarapé Bahia deposits: Implications for the genesis of the iron oxide copper-gold deposits in the Carajás Province, Brazil. Econ. Geol. 114, 697–718. https://doi.org/10.5382/econgeo.4659

Melo, G.H.C. de, Monteiro, L.V.S., Xavier, R.P., Moreto, C.P.N., Santiago, E.S.B., Dufrane, S.A., Aires, B., Santos, A.F.F., 2017. Temporal evolution of the giant Salobo IOCG deposit, Carajás Province (Brazil): constraints from paragenesis of hydrothermal alteration and U-Pb geochronology. Miner. Depos. 52, 709–732. https://doi.org/10.1007/s00126-016-0693-5

Montreuil, J.F., Potter, E.G., Corriveau, L., Davis, W.J., 2016. Element mobility patterns in magnetite-group IOCG systems: The Fab IOCG system, Northwest Territories, Canada. Ore Geol. Rev. 72, 562–584. https://doi.org/10.1016/j.oregeorev.2015.08.010

Moreto, C.P.N., Monteiro, L.V.S., Xavier, R.P., Creaser, R.A., DuFrane, S.A., Tassinari, C.C.G., Sato, K., Kemp, A.I.S., Amaral, W.S., 2015. Neoarchean and paleoproterozoic iron oxide-copper-gold events at the sossego deposit, Carajás Province, Brazil: Re-Os and U-Pb geochronological evidence. Econ. Geol. 110. https://doi.org/10.2113/econgeo.110.3.809

Nadoll, P., Angerer, T., Mauk, J.L., French, D., Walshe, J., 2014. The chemistry of hydrothermal magnetite: A review. Ore Geol. Rev. 61, 1–32. https://doi.org/10.1016/j.oregeorev.2013.12.013

Nadoll, P., Mauk, J.L., Leveille, R.A., Koenig, A.E., 2015. Geochemistry of magnetite from porphyry Cu and skarn deposits in the southwestern United States. Miner. Depos. 50, 493–515. https://doi.org/10.1007/s00126-014-0539-y

Pidgeon, R.T., Macambira, M.J.B., Lafon, J.M., 2000. Th-U-Pb isotopic systems and internal structures of complex zircons from an enderbite from the Pium Complex, Carajas Province, Brazil: Evidence for the ages of granulite facies metamorphism and the protolith of the enderbite. Chem. Geol. 166, 159–171. https://doi.org/10.1016/S0009-2541(99)00190-4

Pinheiro, R.V.L., Holdsworth, R.E., 2000. Eevolução tectonoestratigráfica dos sistemas transcorrentes Carajás e cinzento, Cinturão Itacaiúnas, na borda leste do Craton

Amazónico, Pará. Rev. Bras. Geociências 30, 597–606. https://doi.org/10.1063/1.2756072

Pollard, P.J., 2006. An intrusion-related origin for Cu-Au mineralization in iron oxide-copper-gold (IOCG) provinces. Miner. Depos. 41, 179–187. https://doi.org/10.1007/s00126-006-0054-x

Pollard, P.J., Taylor, R.G., Peters, L., Matos, F., Freitas, C., Saboia, L., Huhn, S., 2018. Ar- 39 Ar dating of Archean iron oxide Cu-Au and Paleoproterozoic granite-related Cu-Au deposits in the Carajás Mineral Province , Brazil : implications for genetic models. Miner. Depos. https://doi.org/10.1007/s00126-018-0809-1

Requia, K., Stein, H., Fontboté, L., Chiaradia, M., 2003. Re-Os and Pb-Pb geochronology of the Archean Salobo iron oxide copper-gold deposit, Carajás mineral province, northern Brazil. Miner. Depos. 38, 727–738. https://doi.org/10.1007/s00126-003-0364-1

Richards, J.P., Mumin, A.H., 2013. Magmatic-hydrothermal processes within an evolving Earth: Iron oxide-copper-gold and porphyry Cu ± Mo ± Au deposits. Geology 41, 767–770. https://doi.org/10.1130/G34275.1

Rojas, P.A., Barra, F., Deditius, A., Reich, M., Simon, A., Roberts, M., Rojo, M., 2018. New contributions to the understanding of Kiruna-type iron oxide-apatite deposits revealed by magnetite ore and gangue mineral geochemistry at the El Romeral deposit, Chile. Ore Geol. Rev. 93, 413–435. https://doi.org/10.1016/j.oregeorev.2018.01.003

Rudnick, R.L., Gao, S., 2003. Composition of the Continental Crust. Treatise on Geochemistry 3, 1–64. https://doi.org/10.1016/B978-0-08-095975-7.00301-6

Rye, R.O., 1993. The Evolution of Magmatic Fluids in the Epithermal Environment: The Stable Isotope Perspective. Econ. Geol. 88, 733–753. https://doi.org/10.2113/gsecongeo.88.3.733

Schlegel, T.U., Wagner, T., Boyce, A., Heinrich, C.A., 2017. A magmatic source of hydrothermal sulfur for the Prominent Hill deposit and associated prospects in the Olympic iron oxide copper-gold (IOCG) province of South Australia. Ore Geol. Rev. 89, 1058–1090. https://doi.org/10.1016/j.oregeorev.2016.09.002

Schutesky, M.E.D.G., Gouveia de Oliveira, C., *accepted*. From the roots to the roof – A new view of The Carajás IOCG Mineral System. Ore Geol. Rev.

Sillitoe, R.H., 2003. Iron oxide-copper-gold deposits: An Andean view. Miner. Depos. 38, 787–812. https://doi.org/10.1007/s00126-003-0379-7

Storey, C.D., Smith, M.P., 2017. Metal source and tectonic setting of iron oxide-copper-gold (IOCG) deposits: Evidence from an in situ Nd isotope study of titanite from Norrbotten, Sweden. Ore Geol. Rev. 81, 1287–1302. https://doi.org/10.1016/j.oregeorev.2016.08.035

Sun, W., Arculus, R.J., Kamenetsky, V.S., Binns, R.A., 2004. Release of gold-bearing fluids in convergent margin magmas prompted by magnetite crystallization. Nature 431, 975–978. https://doi.org/10.1038/nature02972

Sun, W., Huang, R. Fang, Li, H., Hu, Y. bin, Zhang, C. chan, Sun, S. Jun, Zhang, L. Peng, Ding, X., Li, C. Ying, Zartman, R.E., Ling, M. xing, 2015. Porphyry deposits and oxidized magmas. Ore Geol. Rev. 65, 97–131. https://doi.org/10.1016/j.oregeorev.2014.09.004

Sun, W.D., Liang, H.Y., Ling, M.X., Zhan, M.Z., Ding, X., Zhang, H., Yang, X.Y., Li, Y.L., Ireland, T.R., Wei, Q.R., Fan, W.M., 2013. The link between reduced porphyry copper deposits and oxidized magmas. Geochim. Cosmochim. Acta 103, 263–275. https://doi.org/10.1016/j.gca.2012.10.054

Tassinari, C.C.G., Mellito, K.M., Babinski, M., 2003. Age and origin of the Cu (Au-Mo-Ag) Salobo 3A ore deposit, Carajas Mineral Province, Amazonian Craton, northern Brazil. Episodes 26, 2–9.

Tavares, F.M., Trouw, R.A.J., da Silva, C.M.G., Justo, A.P., Oliveira, J.K.M., 2018. The multistage tectonic evolution of the northeastern Carajás Province, Amazonian Craton, Brazil: revealing complex structural patterns. J. South Am. Earth Sci. 88, 238–252. https://doi.org/10.1016/j.jsames.2018.08.024

Urai, J.L., Means, W.D., Lister, G.S., 1986. Dynamic recrystallization of minerals, Series, v. ed. Mineral and rock deformation: Laboratory studies: American Geophysical Union, Geophysical Monograph. https://doi.org/10.1029/gm036p0161

VALE, 2012. Vale obtains operation license for Salobo. [WWW Document]. URL

http://saladeimprensa.vale.com/en/release/interna.asp?id=22000

Vasquez, M.L., Da Rosa-Costa, L.T., Silva, C., Ricci, P., Barbosa, J., Klein, E., Lopes, E., Macambira, E., Chaves, C., Carvalho, J., Oliveira, J., Anjos, G., Silva, H., 2008. Geologia e Recursos Minerais do Estado do Pará: Sistema de Informações Geográficas - SIG: texto explicativo dos mapas Geológico e Tectônico e de Recursos Minerais do Estado do Pará. Organizadores, Marcelo Lacerda Vasquez, Lúcia Travassos da Rosa-Costa. CPRM, Belém.

Vieira, L.V., Schutesky, M.E.D.G., Campo, Y.T.R., Gouveia de Oliveira, C., 2019. A review of the hydrothermal alteration stages in the giant metamorphosed IOCG Salobo deposit, Carajás Mineral Province, Brazil. *Unpublished thesis.* Universidade de Brasília.

Vigneresse, J.L., Truche, L., Richard, A., 2019. How do metals escape from magmas to form porphyry-type ore deposits? Ore Geol. Rev. 105, 310–336. https://doi.org/10.1016/j.oregeorev.2018.12.016

Wang, C., Shao, Y., Zhang, X., Dick, J., Liu, Z., 2018. Trace Element Geochemistry of Magnetite: Implications for Ore Genesis of the Huanggangliang Sn-Fe Deposit, Inner Mongolia, Northeastern China. Minerals 8, 195. https://doi.org/10.3390/min8050195

Wen, G., Li, J., Hofstra, A.H., Koenig, A.E., Lowers, H.A., Adams, D., 2017. Hydrothermal reequilibration of igneous magnetite in altered granitic plutons and its implications for magnetite classification schemes : Insights from the Handan-Xingtai iron district, North China Craton. Geochim. Cosmochim. Acta 213, 255–270. https://doi.org/10.1016/j.gca.2017.06.043

Whitehouse, M.J., Kamber, B.S., Fedo, C.M., Lepland, A., 2005. Integrated Pb- and S-isotope investigation of sulphide minerals from the early Archaean of southwest Greenland. Chem. Geol. 222, 112–131. https://doi.org/10.1016/j.chemgeo.2005.06.004

Williams, P.J., Barton, M.D., Johnson, D.A., Fontboté, L., De Haller, A., Mark, G., Oliver, N.H.S., Marschik, R., 2005. Iron oxide copper-gold deposits: Geology, space-time distribution, and possible modes of origin. Econ. Geol. Anniversar, 371–405. https://doi.org/10.5382/AV100.13

Williams, P.J., Kendrick, M.A., Xavier, R.P., 2010. Sources of Ore Fluid Components in IOCG Deposits. PGC Publ. 3, 107–116.

Xavier, R.P., Monteiro, L.V.S., Moreto, C.P.N., Pestilho, A.L.S., Melo, G.H.C. De, Da Silva, M.A.D., Aires, B., Ribeiro, C., Silva, F.H.F. e, 2012. The Iron Oxide Copper-Gold Systems of the Carajás Mineral Province, Brazil. Econ. Geol. 1–22. https://doi.org/https://doi.org/10.5382/SP.16.17

Conclusões

A magnetita do depósito Salobo IOCG cristalizou em três texturas diferentes em relação aos estágios de mineralização: *brecha de magnetita* – Mgt tipo I, *brecha de calcopirita* – Mgt tipo II e *xisto de magnetita* – Mgt tipo III. A mineralização singenética primária foi formada a partir de um fluido magmático sem influência de condições atmosféricas ou crustais oxidantes, gerando a *magnetita maciça* – Mgt tipo I (alteração Ca-Fe) e a *magnetita em brecha* – Mgt tipo II (mineralização Cu-Au), ambas relacionadas ao evento magmático-hidrotermal em ~ 2,75 - 2,73 Ga.

A assinatura do elemento traço de magnetita assim como o total espectro de isótopos de enxofre dos sulfetos durante o evento magmático-hidrotermal, podem ser explicados pela primeira cristalização de magnetita, cujo fracionamento e saturação desencadeou a redução de sulfato, permitindo a precipitação de sulfetos de Cu-Fe. Além disso, algumas substituições de pirita sugerem que parte da cristalização da calcopirita poderia ter sido conduzida por um fluido de magma oxidado rico em Cu, o qual reagiu com um Fe redutor da pirita inicial, contribuindo para o grau de Cu em Salobo.

Um metamorfismo subsequente relacionado ao emplacamento do Granito Old Salobo, devido à reativação da Zona de Cisalhamento de Cinzento em ~ 2,5 Ga gerou a magnetita recristalizada granoblástica em *xistos de magnetita* – Mgt tipo III, que posteriormente durante o Paleoproteozoico foi submetida a uma remobilização e reconcentração de enxofre, resultando em veios discordantes de bornita, calcocita e digenita que cortam a foliação dos xistos, e texturas de exsoluções de calcocita-covelita em bornita.

Assim, embora a principal mineralização de Cu caracterizada por assembleias de sulfetos de Cu (bornita, calcocita e digenita) e magnetita, esteja relacionada aos eventos de metamorfismo e remobilização, a mineralização primaria de Cu em Salobo foi desenvolvida durante o evento magmático-hidrotermal numa brecha de calcopirita rica em sulfetos de Cu, a qual foi submetida ao metamorfismo, resultando na assembleia "incomum" do minério característica de Salobo, dominada por uma associação de magnetita-bornita-calcococita.

Os dados fornecem uma contribuição na compreensão dos processos que levaram à formação do minério. A distribuição da química de magnetita em diagramas discriminantes não permite uma clara distinção enquanto a origem de depósito, porém mostram que os diferentes tipos de magnetita guardam uma assinatura geoquímica similar apesar dos distintos eventos geológicos-metalogenéticos aos quais estão associados. Desta maneira, a Magnetita tipo III resultou de uma recristalização dos tipos prévios de magnetita tipo I e II. Com base nos resultados de isótopos de enxofre e a relações texturais dos sulfetos analisados se relaciona a origem do conteúdo de Cu a uma fonte de enxofre magmático-hidrotermal de alta temperatura que evoluiu ao longo de vias oxidantes e redutoras durante os estágios de mineralização sem contribuições externas de enxofre. Em conjunto, nossos resultados sugerem um modelo de formação de minério do tipo IOCG que envolve processos semelhantes aos que ocorrem em sistemas magmático-hidrotermais de alta temperatura como pórfiros, denominados "crise da magnetita", contribuindo para a compreensão da gênese da mineralização em depósitos do tipo IOCG.

Referências

Acosta-Góngora, P., Gleeson, S.A., Samson, I.M., Corriveau, L., Ootes, L., Jackson, S.E., Taylor, B.E., Girard, I., 2018. Origin of sulfur and crustal recycling of copper in polymetallic (Cu-Au-Co-Bi-U ± Ag) iron-oxide-dominated systems of the Great Bear Magmatic Zone, NWT, Canada. Miner. Depos. 53, 353–376. https://doi.org/10.1007/s00126-017-0736-6

Avelar, V.G., Lafon, J.M., Correia Jr., F.C., Macambira, E.M.B., 1999. O magmatismo arqueano da região de Tucumã - Província Mineral De Carajás: Novos resultados geocronológicos. Rev. Bras. Geociências 29, 453–460.

Barton, M.D., 2014. Iron Oxide(-Cu-Au-REE-P-Ag-U-Co) Systems, 2nd ed, Treatise on Geochemistry: Second Edition. Elsevier Ltd. https://doi.org/10.1016/B978-0-08-095975-7.01123-2

Biagioni, C., Pasero, M., 2014. The systematics of the spinel-type minerals: An overview. Am. Mineral. 99, 1254–1264. https://doi.org/10.2138/am.2014.4816

Broughm, S.G., Hanchar, J.M., Tornos, F., Westhues, A., Attersley, S., 2017. Mineral chemistry of magnetite from magnetite-apatite mineralization and their host rocks: examples from Kiruna, Sweden, and El Laco, Chile. Miner. Depos. 52, 1223–1244. https://doi.org/10.1007/s00126-017-0718-8

Bühn, B., Santos, R. V., Dardenne, M.A., de Oliveira, C.G., 2012. Mass-dependent and mass-independent sulfur isotope fractionation (δ34S and δ33S) from Brazilian Archean and Proterozoic sulfide deposits by laser ablation multi-collector ICP-MS. Chem. Geol. 312–313, 163–176. https://doi.org/10.1016/j.chemgeo.2012.04.003

Chen, H., 2013. External sulphur in IOCG mineralization: Implications on definition and classification of the IOCG clan. Ore Geol. Rev. 51, 74–78. https://doi.org/10.1016/j.oregeorev.2012.12.002

Dare, S.A.S., Barnes, S.J., Beaudoin, G., Méric, J., Boutroy, E., Potvin-Doucet, C., 2014. Trace elements in magnetite as petrogenetic indicators. Miner. Depos. 49, 785–796. https://doi.org/10.1007/s00126-014-0529-0

Deditius, A.P., Reich, M., Simon, A.C., Suvorova, A., Knipping, J., Roberts, M.P.,

Rubanov, S., Dodd, A., Saunders, M., 2018. Nanogeochemistry of hydrothermal magnetite. Contrib. to Mineral. Petrol. 173, 1–20. https://doi.org/10.1007/s00410-018-1474-1

Delinardo da Silva, M.A., 2014. Metatexitos e Diatexitos do Complexo Xingu na região de Canaã dos Carajás: Implicações para a evolução mesoarqueana do domínio Carajás. Universidade Estadual de Campinas, Brazil.

Dmitrijeva, M., Ehrig, K.J., Ciobanu, C.L., Cook, N.J., Verdugo-Ihl, M.R., Metcalfe, A. V., 2019. Defining IOCG signatures through compositional data analysis: A case study of lithogeochemical zoning from the Olympic Dam deposit, South Australia. Ore Geol. Rev. 105, 86–101. https://doi.org/10.1016/j.oregeorev.2018.12.013

DOCEGEO, 1988. Revisão litoestratigráfica da Província Mineral de Carajás - Litoestratigrafia e principais depósitos minerais. Congr. Bras. Geol. 35th, 11–54.

Droop, G.T.R., 1987. A general equation for estimating Fe 3+ concentrations in ferromagnesian silicates and oxides from microprobe analyses, using stoichiometric criteria. Mineral. Mag. 51, 431–435. https://doi.org/10.1180/minmag.1987.051.361.10

Dupuis, C., Beaudoin, G., 2011. Discriminant diagrams for iron oxide trace element fingerprinting of mineral deposit types. Miner. Depos. 46, 319–335. https://doi.org/10.1007/s00126-011-0334-y

Feio, G.R.L., Dall'Agnol, R., Dantas, E.L., Macambira, M.J.B., Santos, J.O.S., Althoff, F.J., Soares, J.E.B., 2013. Archean granitoid magmatism in the Canaã dos Carajás area: Implications for crustal evolution of the Carajás province, Amazonian craton, Brazil. Precambrian Res. 227, 157–185. https://doi.org/10.1016/j.precamres.2012.04.007

Gelcich, S., Davis, D.W., Spooner, E.T.C., 2005. Testing the apatite-magnetite geochronometer: U-Pb and 40Ar/ 39Ar geochronology of plutonic rocks, massive magnetite-apatite tabular bodies, and IOCG mineralization in Northern Chile. Geochim. Cosmochim. Acta 69, 3367–3384. https://doi.org/10.1016/j.gca.2004.12.020

Gleeson, S.A., Smith, M.P., 2009. The sources and evolution of mineralising fluids in iron oxide-copper-gold systems, Norrbotten, Sweden: Constraints from Br/Cl ratios

and stable Cl isotopes of fluid inclusion leachates. Geochim. Cosmochim. Acta 73, 5658–5672. https://doi.org/10.1016/j.gca.2009.06.005

Groves, D.I., Bierlein, F.P., Meinert, L.D., Hitzman, M.W., 2010. Iron Oxide Copper-Gold (IOCG) Deposits through Earth History: Implications for Origin, Lithospheric Setting, and Distinction from Other Epigenetic Iron Oxide Deposits. Econ. Geol. 105, 641–654. https://doi.org/10.2113/gsecongeo.105.3.641

Halevy, I., Johnston, D.T., Schrag, D.P., 2010. Explaining the Structure of the Archean Mass-Independent Sulfur Isotope Record, Science. https://doi.org/10.1192/bjp.177.1.47

Hitzman, M.W., Oreskes, N., Einaudi, M.T., 1992. Geological characteristics and tectonic setting of proterozoic iron oxide (CuUAuREE) deposits. Precambrian Res. 58, 241–287. https://doi.org/10.1016/0301-9268(92)90121-4

Huang, X., Boutroy, É., Makvandi, S., Beaudoin, G., Corriveau, L., Toni, A.F. De, 2019. Trace element composition of iron oxides from IOCG and IOA deposits : relationship to hydrothermal alteration and deposit subtypes. Miner. Depos. 54, 525–552.

Huang, X.W., Beaudoin, G., 2019. Textures and chemical compositions of magnetite from iron oxide copper-gold (IOCG) and kiruna-type iron oxide-apatite (IOA) deposits and their implications for ore genesis and magnetite classification schemes. Econ. Geol. 114, 953–979. https://doi.org/10.5382/econgeo.4651

Huhn Bacelar, S.R., 1996. São os depósitos cupríferos de Carajás do tipo Cu-Au-U-(ETR)?, in: Sociedade Brasileira de Geologia, N.N. (Ed.), Boletim de Resumos Expandidos e Guia de Excursões. Belém - Pará, pp. 140–143.

Jenner, F.E., O'Neill, H.S.C., Arculus, R.J., Mavrogenes, J.A., 2010. The magnetite crisis in the evolution of arc-related magmas and the initial concentration of Au, Ag and Cu. J. Petrol. 51, 2445–2464. https://doi.org/10.1093/petrology/egq063

Johnston, D.T., 2011. Multiple sulfur isotopes and the evolution of Earth's surface sulfur cycle. Earth-Science Rev. 106, 161–183. https://doi.org/10.1016/j.earscirev.2011.02.003

Knipping, J.L., Bilenker, L.D., Simon, A.C., Reich, M., Barra, F., Deditius, A.P., Wälle,

M., Heinrich, C.A., Holtz, F., Munizaga, R., 2015. Trace elements in magnetite from massive iron oxide-apatite deposits indicate a combined formation by igneous and magmatic-hydrothermal processes. Geochim. Cosmochim. Acta 171, 15–38. https://doi.org/10.1016/j.gca.2015.08.010

Lindenmayer, Z.G., 1990. Salobo sequence, Carajás, Brasil: Geology, geochemistry and metamorphism. Western University.

Lindenmayer, Z.G., Teixeira, J.B.G., 1999. Ore genesis at the Solobo copper deposit, Serra dos Carajás. Base Met. Depos. Brazil 33–43.

Machado, N., Lindenmayer, Z., Krogh, T.E., Lindenmayer, D., 1991. U-Pb geochronology of Archean magmatism and basement reactivation in the Carajás area, Amazon shield, Brazil. Precambrian Res. 49, 329–354. https://doi.org/10.1016/0301-9268(91)90040-H

Melo, G.H.C. de, Monteiro, L.V.S., Xavier, R.P., Moreto, C.P.N., Santiago, E., 2019. Tracing fluid sources for the salobo and Igarapé Bahia deposits: Implications for the genesis of the iron oxide copper-gold deposits in the Carajás Province, Brazil. Econ. Geol. 114, 697–718. https://doi.org/10.5382/econgeo.4659

Melo, G.H.C. de, Monteiro, L.V.S., Xavier, R.P., Moreto, C.P.N., Santiago, E.S.B., Dufrane, S.A., Aires, B., Santos, A.F.F., 2017. Temporal evolution of the giant Salobo IOCG deposit, Carajás Province (Brazil): constraints from paragenesis of hydrothermal alteration and U-Pb geochronology. Miner. Depos. 52, 709–732. https://doi.org/10.1007/s00126-016-0693-5

Montreuil, J.F., Potter, E.G., Corriveau, L., Davis, W.J., 2016. Element mobility patterns in magnetite-group IOCG systems: The Fab IOCG system, Northwest Territories, Canada. Ore Geol. Rev. 72, 562–584. https://doi.org/10.1016/j.oregeorev.2015.08.010

Moreto, C.P.N., Monteiro, L.V.S., Xavier, R.P., Creaser, R.A., DuFrane, S.A., Tassinari, C.C.G., Sato, K., Kemp, A.I.S., Amaral, W.S., 2015. Neoarchean and paleoproterozoic iron oxide-copper-gold events at the sossego deposit, Carajás Province, Brazil: Re-Os and U-Pb geochronological evidence. Econ. Geol. 110. https://doi.org/10.2113/econgeo.110.3.809

Nadoll, P., Angerer, T., Mauk, J.L., French, D., Walshe, J., 2014. The chemistry of

hydrothermal magnetite: A review. Ore Geol. Rev. 61, 1–32. https://doi.org/10.1016/j.oregeorev.2013.12.013

Nadoll, P., Mauk, J.L., Leveille, R.A., Koenig, A.E., 2015. Geochemistry of magnetite from porphyry Cu and skarn deposits in the southwestern United States. Miner. Depos. 50, 493–515. https://doi.org/10.1007/s00126-014-0539-y

Pidgeon, R.T., Macambira, M.J.B., Lafon, J.M., 2000. Th-U-Pb isotopic systems and internal structures of complex zircons from an enderbite from the Pium Complex, Carajas Province, Brazil: Evidence for the ages of granulite facies metamorphism and the protolith of the enderbite. Chem. Geol. 166, 159–171. https://doi.org/10.1016/S0009-2541(99)00190-4

Pinheiro, R.V.L., Holdsworth, R.E., 2000. Eevolução tectonoestratigráfica dos sistemas transcorrentes Carajás e cinzento, Cinturão Itacaiúnas, na borda leste do Craton Amazónico, Pará. Rev. Bras. Geociências 30, 597–606. https://doi.org/10.1063/1.2756072

Pollard, P.J., 2006. An intrusion-related origin for Cu-Au mineralization in iron oxide-copper-gold (IOCG) provinces. Miner. Depos. 41, 179–187. https://doi.org/10.1007/s00126-006-0054-x

Pollard, P.J., Taylor, R.G., Peters, L., Matos, F., Freitas, C., Saboia, L., Huhn, S., 2018. Ar- 39 Ar dating of Archean iron oxide Cu-Au and Paleoproterozoic granite-related Cu-Au deposits in the Carajás Mineral Province , Brazil : implications for genetic models. Miner. Depos. https://doi.org/10.1007/s00126-018-0809-1

Requia, K., Stein, H., Fontboté, L., Chiaradia, M., 2003. Re-Os and Pb-Pb geochronology of the Archean Salobo iron oxide copper-gold deposit, Carajás mineral province, northern Brazil. Miner. Depos. 38, 727–738. https://doi.org/10.1007/s00126-003-0364-1

Richards, J.P., Mumin, A.H., 2013. Magmatic-hydrothermal processes within an evolving Earth: Iron oxide-copper-gold and porphyry Cu ± Mo ± Au deposits. Geology 41, 767–770. https://doi.org/10.1130/G34275.1

Rojas, P.A., Barra, F., Deditius, A., Reich, M., Simon, A., Roberts, M., Rojo, M., 2018. New contributions to the understanding of Kiruna-type iron oxide-apatite deposits revealed by magnetite ore and gangue mineral geochemistry at the El Romeral

deposit, Chile. Ore Geol. Rev. 93, 413–435. https://doi.org/10.1016/j.oregeorev.2018.01.003

Rudnick, R.L., Gao, S., 2003. Composition of the Continental Crust. Treatise on Geochemistry 3, 1–64. https://doi.org/10.1016/B978-0-08-095975-7.00301-6

Rye, R.O., 1993. The Evolution of Magmatic Fluids in the Epithermal Environment: The Stable Isotope Perspective. Econ. Geol. 88, 733–753. https://doi.org/10.2113/gsecongeo.88.3.733

Schlegel, T.U., Wagner, T., Boyce, A., Heinrich, C.A., 2017. A magmatic source of hydrothermal sulfur for the Prominent Hill deposit and associated prospects in the Olympic iron oxide copper-gold (IOCG) province of South Australia. Ore Geol. Rev. 89, 1058–1090. https://doi.org/10.1016/j.oregeorev.2016.09.002

Schutesky, M.E.D.G., Gouveia de Oliveira, C., n.d. From the roots to the roof – A new view of The Carajás IOCG Mineral System. Ore Geol. Rev.

Sillitoe, R.H., 2003. Iron oxide-copper-gold deposits: An Andean view. Miner. Depos. 38, 787–812. https://doi.org/10.1007/s00126-003-0379-7

Storey, C.D., Smith, M.P., 2017. Metal source and tectonic setting of iron oxide-copper-gold (IOCG) deposits: Evidence from an in situ Nd isotope study of titanite from Norrbotten, Sweden. Ore Geol. Rev. 81, 1287–1302. https://doi.org/10.1016/j.oregeorev.2016.08.035

Sun, W., Arculus, R.J., Kamenetsky, V.S., Binns, R.A., 2004. Release of gold-bearing fluids in convergent margin magmas prompted by magnetite crystallization. Nature 431, 975–978. https://doi.org/10.1038/nature02972

Sun, W., Huang, R. Fang, Li, H., Hu, Y. bin, Zhang, C. chan, Sun, S. Jun, Zhang, L. Peng, Ding, X., Li, C. Ying, Zartman, R.E., Ling, M. xing, 2015. Porphyry deposits and oxidized magmas. Ore Geol. Rev. 65, 97–131. https://doi.org/10.1016/j.oregeorev.2014.09.004

Sun, W.D., Liang, H.Y., Ling, M.X., Zhan, M.Z., Ding, X., Zhang, H., Yang, X.Y., Li, Y.L., Ireland, T.R., Wei, Q.R., Fan, W.M., 2013. The link between reduced porphyry copper deposits and oxidized magmas. Geochim. Cosmochim. Acta 103, 263–275. https://doi.org/10.1016/j.gca.2012.10.054

Tassinari, C.C.G., Mellito, K.M., Babinski, M., 2003. Age and origin of the Cu (Au-Mo-Ag) Salobo 3A ore deposit, Carajas Mineral Province, Amazonian Craton, northern Brazil. Episodes 26, 2–9.

Tavares, F.M., Trouw, R.A.J., da Silva, C.M.G., Justo, A.P., Oliveira, J.K.M., 2018. The multistage tectonic evolution of the northeastern Carajás Province, Amazonian Craton, Brazil: revealing complex structural patterns. J. South Am. Earth Sci. 88, 238–252. https://doi.org/10.1016/j.jsames.2018.08.024

Urai, J.L., Means, W.D., Lister, G.S., 1986. Dynamic recrystallization of minerals, Series, v. ed. Mineral and rock deformation: Laboratory studies: American Geophysical Union, Geophysical Monograph. https://doi.org/10.1029/gm036p0161

VALE, 2012. Vale obtains operation license for Salobo. [WWW Document]. URL http://saladeimprensa.vale.com/en/release/interna.asp?id=22000

Vasquez, M.L., Da Rosa-Costa, L.T., Silva, C., Ricci, P., Barbosa, J., Klein, E., Lopes, E., Macambira, E., Chaves, C., Carvalho, J., Oliveira, J., Anjos, G., Silva, H., 2008. Geologia e Recursos Minerais do Estado do Pará: Sistema de Informações Geográficas - SIG: texto explicativo dos mapas Geológico e Tectônico e de Recursos Minerais do Estado do Pará. Organizadores, Marcelo Lacerda Vasquez, Lúcia Travassos da Rosa-Costa. CPRM, Belém.

Vieira, L.V., Schutesky, M.E.D.G., Campo, Y.T.R., Gouveia de Oliveira, C., 2019. A review of the hydrothermal alteration stages in the giant metamorphosed IOCG Salobo deposit, Carajás Mineral Province, Brazil. Universidade de Brasília.

Vigneresse, J.L., Truche, L., Richard, A., 2019. How do metals escape from magmas to form porphyry-type ore deposits? Ore Geol. Rev. 105, 310–336. https://doi.org/10.1016/j.oregeorev.2018.12.016

Wang, C., Shao, Y., Zhang, X., Dick, J., Liu, Z., 2018. Trace Element Geochemistry of Magnetite: Implications for Ore Genesis of the Huanggangliang Sn-Fe Deposit, Inner Mongolia, Northeastern China. Minerals 8, 195. https://doi.org/10.3390/min8050195

Wen, G., Li, J., Hofstra, A.H., Koenig, A.E., Lowers, H.A., Adams, D., 2017. Hydrothermal reequilibration of igneous magnetite in altered granitic plutons and its implications for magnetite classification schemes : Insights from the Handan-

Xingtai iron district, North China Craton. Geochim. Cosmochim. Acta 213, 255–270. https://doi.org/10.1016/j.gca.2017.06.043

Whitehouse, M.J., Kamber, B.S., Fedo, C.M., Lepland, A., 2005. Integrated Pb- and S-isotope investigation of sulphide minerals from the early Archaean of southwest Greenland. Chem. Geol. 222, 112–131. https://doi.org/10.1016/j.chemgeo.2005.06.004

Williams, P.J., Barton, M.D., Johnson, D.A., Fontboté, L., De Haller, A., Mark, G., Oliver, N.H.S., Marschik, R., 2005. Iron oxide copper-gold deposits: Geology, space-time distribution, and possible modes of origin. Econ. Geol. Anniversar, 371–405. https://doi.org/10.5382/AV100.13

Williams, P.J., Kendrick, M.A., Xavier, R.P., 2010. Sources of Ore Fluid Components in IOCG Deposits. PGC Publ. 3, 107–116.

Xavier, R.P., Monteiro, L.V.S., Moreto, C.P.N., Pestilho, A.L.S., Melo, G.H.C. De, Da Silva, M.A.D., Aires, B., Ribeiro, C., Silva, F.H.F. e, 2012. The Iron Oxide Copper-Gold Systems of the Carajás Mineral Province , Brazil. Econ. Geol. 1–22. https://doi.org/https://doi.org/10.5382/SP.16.17